

Scientific paper

Synthesis, Characterization and Biological Applications of Substituted Indolo[2,1-b]quinazolin-12(6H)-one Based Rhenium(I) Organometallic Compounds

Aelvish D. Padariya,¹ Nirbhay K. Savaliya,¹ Milan P. Dhaduk,¹ Ravi A. Dabhi,¹ Bhupesh S. Bhatt,¹ Vaibhay D. Bhatt² and Mohan N. Patel^{1,*}

¹ Department of Chemistry, Sardar Patel University, Vallabh Vidyanagar–388 120, Gujarat (India)

² School of Applied Sciences and Technology, Gujarat Technological University, Ahmedabad, (India)

* Corresponding author: E-mail: jeenen@gmail.com

Received: 07-23-2023

Abstract

The Re(I) organometallic compounds [(Re(CO) $_3$ L¹⁻⁶)Cl], where ligands L are tryptanthrin derivatives, prepared and characterized by various spectroscopic techniques. To assess the binding capacities and binding manner, tests of calf thymus DNA under the impact of organometallic complexes were conducted using absorption titration and viscosity measuring techniques. Data from the research mentioned above point to an intercalation type of binding, which was verified by the docking study. Swiss ADME tools were used to carry out an ADME study. The work focuses on computing the molecular orbital energies for the synthesized compounds using the density functional theory (DFT). The compounds were tested against the MCF-7 cell line to determine their anticancer effects. It was observed that their IC50 values were equivalent to those of the standard medication, indicating that they had a similar antiproliferative impact.

Keywords: Re(I) organometallic compounds, DNA and BSA binding, DFT, Molecular docking, ADMET study, Antibacterial activity, Anticancer activity

1. Introduction

Research is heavily focused on creating new, more effective anti-cancer medications because there are drawbacks to present metal-based anticancer drugs like cisplatin. Metal-containing compounds have been investigated recently as prospective possibilities for innovative pharmaceuticals. The finding that apoptosis and the genes that control it considerably impact cancer phenotype has contributed to important improvements in our understanding of cancer biology and genetics.² Tryptanthrin, an alkaloid, and antibiotic has been found to have antibacterial, and anti-tumor activity and has been isolated from various sources including Candida lypolica, higher plants, and marine micro- and macro-organisms.^{3,4} Natural remedies have been used for centuries as sources of treatment and prevention for various illnesses including cancer. The anti-cancer drug paclitaxel was first extracted from Taxus brevifolia and approved by the Food and Drug Analysis for the treatment of several types of cancer.⁵ Schiff base ligands have been extensively explored in coordination

chemistry and are significant in this area because of their stability, chelating properties, and capacity to form complexes with transition metals.^{6,7} Tryptanthrin and its derivatives, due to their broad spectrum of activity against various diseases, have become potential biologically active compounds.⁸ The quinazoline and indole core structures found in tryptanthrin serve as building blocks.⁹ Tryptanthrin's unique indolo[2,1-*b*]quinazoline ring structure has attracted significant attention in chemical research due to its crucial role in the synthesis of natural products, materials, and pharmaceuticals.¹⁰ Many plant species contain tryptanthrin and candidine, phaitanthrins A–E, methylisatoid, and cruciferane (Figure 1).

Nowadays one promising category of synthetic or naturally occurring chemicals that could be used in cancer treatment is quinazoline compounds.¹¹ Tryptanthrin has been investigated for its potential use in cancer therapy due to its antitumor properties.¹² Chemotherapy is the current standard treatment for cancer in clinical settings.^{13,14} However, multidrug resistance affects effectiveness for anticancer medications. One of the most popular

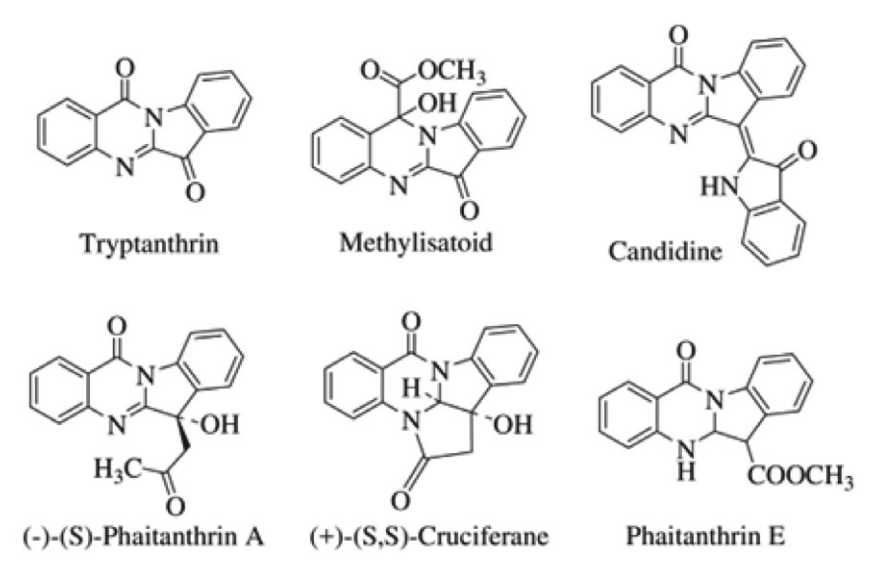


Figure 1. Tryptanthrin and related alkaloids

cytotoxic and antibacterial reagents is a quinazoline alkaloid produced by sublimating natural indigo under reduced pressure.¹⁵

Density functional theory (DFT) has been increasingly popular in biochemical and medicinal research. DFT is being used more and more in these domains to solve a variety of issues. Dipole moments and global characteristics are one of the main areas of interest in this research since they are essential to understanding the reactivity and bioactivity of compounds, especially those designed for biomedical uses. A useful approach for determining the affinities of candidate compounds to their intended targets is molecular docking studies. This approach is crucial for optimizing potential compounds for medication development and for understanding how ligands interact with their target proteins. 16 Additionally, it is crucial for therapeutic development to estimate the lead compounds AD-MET characteristics. These characteristics offer vital information on a drug's absorption, distribution, metabolization, excretion, and potential toxicity. 17,18 Techniques like pharmacokinetic parameter analysis and toxicity evaluation are effective tools in the field of in silico drug design. They allow researchers to examine novel chemicals' physical and chemical properties and gauge their potential toxicity. These techniques are essential for swiftly selecting drugs that have potential for additional preclinical and clinical research.19

Chemotherapy is a widely used treatment option for cancer, but its lack of specificity towards malignant cells can result in adverse side effects and limit its effectiveness. To overcome this limitation, researchers have been working on developing and synthesizing organometallic compounds with therapeutic potential, particularly those with anticancer properties. Platinum complexes, including *cis*-PtX₂L₂, as well as palladacycles, dimeric, trimeric, tetrameric, and heterobimetallic complexes, have been the focus of much research in the field of anticancer drugs. 22

Recent years have seen the development of a variety of Pt(II) compounds containing nitrogen atom donor ligands like alkyl and aryl type amines and imines. Such as azo, hydrazo, pyridine, and pyrimidine derivatives.²³ Few of these complexes have demonstrated effective anticancer capabilities both *in vivo* and *in vitro*. The tryptanthrin Schiff base and substituted phenyl hydrazine synthesized, characterized, and their interactions within DNA and BSA investigated are presented in this study. In order to ascertain mechanism and type of interaction of organometallic complexes with DNA, the molecular docking technique was also used. These findings could potentially increase the development of the novel and effective anticancer agents with additionally improved specificity toward malignant cells.²⁴

2. Experimental Section

2. 1. Materials and Methods

The reagents and solvents employed have high chemical purity and reasonably priced. For spectral measurements, spectroscopic-grade solvents were purchased from Sigma-Aldrich. The following items were acquired from Sigma-Aldrich: isatin, 5-chloroisatin, isatoic anhydride, triethylamine, pentacarbonylchlororhenium(I), dimethyl sulphoxide (DMSO), calf thymus (CT) DNA, and bovine serum albumin (BSA). The SRL was used to purchase the toluene, methanol, and glacial acetic acid. TCI supplied the following: phenylhydrazine hydrochloride, 4-chlorophenylhydrazine hydrochloride, and 2,4-dichlorophenylhydrazine hydrochloride. We purchased Luria broth and ethidium bromide (EtBr) from Hi-media. Using Milli-Q water, all buffers and solutions are created.

Using a deuterated solvent and a Bruker Avance spectrometer the ¹H NMR spectra were measured. The ¹³C NMR spectra were gathered using a Varian Inova spectrometer and a deuterated solvent. Samples were produced as pellets

of potassium bromide (KBr) for the IR spectral analysis, and an Anasys Fourier transform-infrared (FT-IR) spectrophotometer was used to obtain the spectra in the 4000-400 cm⁻¹ range. A EURO EA3000 elemental analyzer was used to ascertain the elemental makeup of C, H, and N. Using a UV-160A UV-visible spectrophotometer (Shimadzu, Kyoto, Japan), the absorption titration was carried out. A Horiba spectrofluorometer was used to conduct a study on the quenching of fluorescence. A specialized tool created to monitor and examine fluorescence phenomena is the Horiba spectrofluorometer. A study conducted on five bacterial cultures, including two Gram-positive bacteria, Staphylococcus aureus (MTCC-3160) and Bacillus subtilis (MTCC-7193), and three Gram-negative bacteria, Serratia marcescens (MTCC-7103), Escherichia coli (MTCC-433), and Pseudomonas aeruginosa (MTCC-1688) was used to evaluate the antimicrobial activity of the synthesized compounds.

2. 2. Synthesis of Ligands and Their Re(I) Organometallic Compounds

2. 1. 1. Synthesis of Substituted Indolo[2,1-*b*] quinazoline-6,12-dione

Substituted isatin (300 mg, 2.04 mmol) was dissolved in toluene (5 mL), and then triethylamine base (0.567 mL, 4.07 mmol) was added. After 10 minutes isatoic anhydride (332 mg, 2.04 mmol) was added to the reaction mixture

followed by reflux for 70–80 min. The substituted in-dolo[2,1-*b*]quinazoline-6,12-dione products were collected, dried, and washed with methanol to remove impurities.

2. 1. 2. Synthesis of Substituted Tryptanthrin Schiff-based Derivatives (L¹–L⁶)

Synthesized product (300 mg, 1.21 mmol) was reacted with substituted phenylhydrazine hydrochloride (261 mg, 2.42 mmol) derivatives by Schiff-base reaction in the presence of methanol (3 mL) and drops of glacial acetic acid (2–3 drops) at room temperature for 180–240 min with stirring. The substituted tryptanthrin Schiff base product ($\mathbf{L^1-L^6}$) was obtained and collected using vacuum filtration. The resultant precipitates were then washed with a small amount of methanol followed by drying.

2. 1. 3. Synthesis of Re(I) Organometallic Complexes C¹-C⁶

Tryptanthrin Schiff base ligands L¹–L⁶ (100 mg, 0.30 mmol) dissolved in toluene and rhenium metal salt (107 mg, 0.30 mmol) were added and refluxed at 95 °C for 8–9 h with vigorous rapid stirring. Then, the reaction mixture was cooled to room temperature. The resulting precipitates were collected, rinsed with a minor amount of toluene and dried. The column chromatography method was used for the purification of these compounds (Scheme 1).

Scheme 1. The scheme for synthesizing $L^1\!-\!L^6$ and $C^1\!-\!C^6$.

2. 3. Characterization of Ligands and Re(I) Complexes

6-(2-Phenylhydrazono)indolo[2,1-b]quinazolin-12(6H)-one (L¹)

Yield: 82.56% (247.68 mg) of canary yellow amorphous solid; m.p. 220 °C; mol. wt.: 338.37 g/mol. Anal. calcd. for C₂₁H₁₄N₄O: C, 74.54; H, 4.17; N, 16.56. Found: C, 74.41; H, 4.01; N, 14.65. ¹H NMR (400 MHz, CDCl₃) δ 12.74 (1H, s, H_{2}), 7.98 (1H, d, J = 7.2 Hz, H_{5}), 7.67 (1H, d, $J = 7.6 \text{ Hz H}_{10}$, 7.43–7.36 (4H, m, H_{3,4,8,9}), 7.25 (1H, d, J =7.6 Hz, H_2), 7.22 (1H, d, J = 7.6 Hz, H_7), 7.21–7.01 (3H, m, $H_{5,6,7}$), 6.97 (1H, d, J = 7.6 Hz, H_{4}), 6.92 (1H, d, J = 8.0 Hz, $H_{8'}$); ¹³C NMR (125 MHz, CDCl₃) δ 159.53 (C₈), 151.38 (C_{16}) , 151.02 (C_{17}) , 145.47 $(C_{2.3})$, 143.58 (C_{20}) , 133.41 (C_4) , 131.80 (C_{12}), 129.67 (C_{11}), 129.49 ($C_{22,24}$), 129.39 (C_{14}), $128.99 (C_5), 126.58 (C_3), 126.26 (C_6), 124.29 (C_{13}), 122.25$ (C_{23}) , 120.48 (C_7) , 117.74 (C_{15}) , 113.47 $(C_{21,25})$; IR (KBr) v 3047 (=C-H)_{stretching}, 1643 (C=O)_{stretching}, 1550 (C=N) stretching, 1465 (C=C)_{ar. stretching}, 1164 (C-N)_{stretching}, 740 $(C-H)_{\text{bending cm}^{-1}}$; MS m/z (%): 338 (100) [M⁺].

8-Chloro-6-(2-phenylhydrazono)indolo[2,1-b] quinazolin-12(6H)-one (L²)

Yield: 85.43% (256.29 mg) of golden yellow amorphous solid; m.p. 260 °C; mol. wt.: 372.81 g/mol. Anal. calcd. for C₂₁H₁₃ClN₄O: C, 67.66; H, 3.51; N, 15.03. Found: C, 67.53; H, 3.65; N, 14.89. 1 H NMR (400 MHz, CDCl₃) δ 12.77 (1H, s, H_{2}), 7.67 (1H, d, J = 7.2 Hz, H_{5}), 7.56 (1H, s, H_{10}), 7.41–7.40 (4H, m, $H_{4,5,7,8}$), 7.24 (1H, d, J = 6.8 Hz, H_2), 7.21 (1H, d, J = 7.6 Hz, H_8), 7.14 (1H, t, J = 7.1 Hz, H_3), 7.12 (1H, t, J = 6.8 Hz, H_4), 6.96 (1H, t, J = 7.6 Hz, H_{6}), 6.85 (1H, d, J = 8.4 Hz, H_{7}); ¹³C NMR (125 MHz, CDCl₃) δ 160.59 (C₈), 151.85 (C₁₆), 151.30 (C₁₇), 145.43 (C_2) , 143.79 (C_{10}) , 143.18 (C_{20}) , 133.47 (C_4) , 131.19 (C_{12}) , 130.07 (C_{13}), 129.51 (C_{14}), 129.04 ($C_{22.24}$), 127.21 (C_{5}), 126.79 (C₃), 126.59 (C₆), 124.43 (C₁₁), 122.01 (C₂₃), 120.48 (C₇), 119.13 (C₁₅), 113.43 (C_{21,25}); IR (KBr) v 3062 (=C-H) stretching, 1635 (C=O)_{stretching}, 1550 (C=N)_{stretching}, 1465 (C=C)_{ar, stretching}, 1164 (C-N)_{stretching}, 655 (C-Cl)_{bending} cm⁻¹; MS m/z (%): 372 (100) [M⁺], 374 [M⁺²].

6-(2-(4-Chlorophenyl)hydrazono)indolo[2,1-*b*] quinazolin-12(6*H*)-one (L³)

Yield: 80.84% (242.52 mg) of bright yellow amorphous solid; m.p. 270 °C; mol. wt.: 372.81 g/mol. Anal. calcd. for $C_{21}H_{13}ClN_4O$: C, 67.66; H, 3.51; N, 15.03. Found: C, 67.79; H, 3.52; N, 14.91. 1H NMR (400 MHz, CDCl₃) δ 13.49 (1H, s, H₂·), 8.53 (1H, d, J = 8.4 Hz, H₅), 8.47 (1H, d, J = 8.0 Hz, H₁₀), 7.87–7.80 (3H, m, H_{2,7,3}), 7.61–7.55 (1H, m, H₈), 7.50–7.45 (3H, m, H_{4,4;5}·), 7.42 (1H, d, J = 7.6 Hz, H₃·), 7.40 (1H, d, J = 6.8 Hz, H₇·), 7.16 (1H, t, J = 7.2 Hz, H₉); 13 C NMR (125 MHz, CDCl₃) δ 160.24 (C₈), 151.88 (C₁₆), 150.75 (C₁₇), 145.31 (C_{2,9}), 141.66 (C₂₀), 133.49 (C₄), 131.17 (C₁₂), 129.71 (C_{11,24,22}), 128.98 (C₁₄), 127.45 (C₂₃), 126.99 (C₅), 125.92 (C₃), 125.11 (C₆), 123.81 (C₁₃), 120.57

(C₇), 118.19 (C_{15,25,21}); IR (KBr) v 3039 (=C-H)_{stretching}, 1674 (C=O)_{stretching}, 1558 (C=N)_{stretching}, 1512 (C-H)_{bending}, 1465 (C=C)_{ar. stretching}, 1164 (C-N)_{stretching}, 655 (C-Cl) _{bending} cm⁻¹; MS m/z (%): 372 (100) [M⁺], 374 [M⁺²].

8-Chloro-6-(2-(4-chlorophenyl)hydrazono) indolo[2,1-*b*]quinazolin-12(6*H*)-one (L⁴)

Yield: 75.62% (226.86 mg) of lemon yellow amorphous solid; m.p. 275 °C; mol. wt.: 407.25 g/mol. Anal. calcd. for C₂₁H₁₂Cl₂N₄O: C, 61.39; H, 2.97; N, 13.76. Found: C, 61.76; H, 2.84; N, 13.90. ¹H NMR (400 MHz, CDCl₃) δ 13.39 (1H, s, H_{2}), 8.54 (1H, d, J = 8.0 Hz, H_{5}), 8.43 (1H, d, $J = 8.0 \text{ Hz}, H_7$, 8.04 (1H, s, H_{10}), 7.82–7.74 (2H, m, $H_{3.4}$), 7.56 (1H, d, J = 7.6 Hz, H₂), 7.51 (1H, d, J = 8.4 Hz, H₈), 7.45–7.29 (4H, m, $H_{4.5.7.8}$); ¹³C NMR (125 MHz, CDCl₃) δ 162.05 (C₈), 153.95 (C₁₆), 152.83 (C₁₇), 145.87 (C₂), 143.51 (C_{10}) , 142.25 (C_{20}) , 133.85 (C_4) , 131.39 (C_{12}) , 130.62 (C_{13}) , 129.79 ($C_{24,24}$), 129.20 (C_{14}), 127.64 (C_{23}), 127.04 (C_{5}), $125.62 (C_3), 124.77 (C_6), 122.51 (C_{11}), 120.59 (C_7), 119.04$ $(C_{21,25})$, 117.89 (C_{15}) ; IR (KBr) v 3055 $(=C-H)_{\text{stretching}}$ 1643 (C=O)_{stretching}, 1558 (C=N)_{stretching}, 1504 (C-H)_{bend} ing, 1465 (C=C)_{ar. stretching}, 817 (C-Cl)_{bending} cm⁻¹; MS m/z (%): 406 (100) [M⁺], 408 [M⁺²], 412 [M⁺⁴].

6-(2-(2,4-Dichlorophenyl)hydrazono)indolo[2,1-*b*] quinazolin-12(6*H*)-one (L⁵)

Yield: 81.44% (244.32 mg) of honey yellow amorphous solid; m.p. 265 °C; mol. wt.: 407.25 g/mol. Anal. calcd. for C₂₁H₁₂Cl₂N₄O: C, 61.39; H, 2.97; N, 13.76. Found: C, 62.08; H, 2.86; N, 13.89. 1 H NMR (400 MHz, CDCl₃) δ 12.99 (1H, s, H_{2}), 7.81 (1H, d, J = 7.2 Hz, H_{5}), 7.68 (1H, d, $J = 7.2 \text{ Hz}, H_{10}$, 7.57 (1H, s, H_{7}), 7.51–7.43 (3H, m, $H_{3.4.8}$), 7.40 (1H, d, J = 7.6 Hz, H₂), 7.32 (1H, d, J = 6.4 Hz, H₇), 7.30 (1H, d, J = 6.8 Hz, H_{5}), 7.14 (1H, t, J = 7.2 Hz, H_{9}), 6.93 (1H, d, J = 8.0 Hz, H_4); ¹³C NMR (125 MHz, CDCl₃) δ 161.42 (C₈), 155.82 (C₁₆), 153.83 (C₁₇), 148.09 (C_{2.10}), 147.31 (C_{20}), 133.76 (C_4), 131.98 ($C_{22,12}$), 130.79 (C_{11}), 130.58 (C₁₄), 129.14 (C₂₄), 128.55 (C₅), 126.84 (C₃), 126.14 $(C_{6,21})$, 125.33 (C_{13}) , 122.47 (C_{23}) , 120.48 (C_{25}) , 119.51 (C_{15}) , 117.92 (C_7) ; IR (KBr) v 3055 $(=C-H)_{\text{stretching}}$, 1620 (C=O)_{stretching}, 1558 (C=N)_{stretching}, 1512 (C-H)_{bending}, 1465 (C=C)_{ar. stretching}, 1164 (C-N)_{stretching}, 655 (C-Cl)_{bend-} $_{\text{ing}}$ cm⁻¹; MS m/z (%): 406 (100) [M⁺], 408 [M⁺²], 412 $[M^{+4}].$

8-Chloro-6-(2-(2,4-dichlorophenyl)hydrazono) indolo[2,1-*b*]quinazolin-12(6*H*)-one (L⁶)

Yield: 78.38% (235.14 mg) of butter yellow amorphous solid; m.p. 268 °C; mol. wt.: 441.70 g/mol. Anal. calcd. for C₂₁H₁₁Cl₃N₄O: C, 57.11; H, 2.51; N, 12.68. Found: C, 57.23; H, 2.38; N, 12.81. ¹H NMR (400 MHz, CDCl₃) δ 13.47 (1H, s, H₂·), 8.52 (1H, d, J = 8.0 Hz, H₅), 8.47 (1H, d, J = 8.0 Hz, H₇), 7.99 (1H, s, H₁₀), 7.83 (1H, d, J = 7.6 Hz, H₂), 7.71 (1H, d, J = 7.2 Hz, H₈), 7.58 (1H, t, J = 6.8 Hz, H₃), 7.48 (1H, s, H₅·), 7.40 (1H, d, J = 8.4 Hz, H₈·), 7.16 (1H, t, J = 7.2 Hz, H₄), 7.07 (1H, d, J = 7.6 Hz, H₇·); ¹³C

NMR (125 MHz, CDCl₃) δ 160.35 (C₈), 152.51 (C₁₆), 151.25 (C₁₇), 148.15 (C₂), 147.44 (C₂₀), 143.09 (C₁₀), 139.31 (C₄), 138.25 (C₁₂), 136.92 (C₂₂), 133.77 (C₁₃), 132.90 (C₁₄), 132.14 (C₂₄), 132.04 (C₅), 131.91 (C₃), 131.85 (C_{6,21}), 129.18 (C₂₃), 124.85 (C₁₁), 120.52 (C₇), 118.03 (C_{25,15}); IR (KBr) v 3078 (=C-H)_{stretching}, 1627 (C=O)_{stretching}, 1558 (C=N)_{stretching}, 1512 (C-H)_{bending}, 1450 (C=C)_{ar, stretching}, 1172 (C-N)_{stretching}, 655 (C-Cl)_{bending} cm⁻¹; MS m/z (%): 440 (100) [M⁺], 442 [M⁺²], 446 [M⁺⁴], 452 [M⁺⁶].

$[(Re(CO)_3L^1)Cl](C^1)$

Yield: 54.32% (54.32 mg) of caramel brown amorphous solid; m.p. >300 °C; mol. wt.: 644.06 g/mol ($C_{24}H_{14}ClN_4O_4Re$); ¹H NMR (400 MHz, DMSO- d_6) δ 12.75 (1H, s, H₂·), 7.56 (1H, d, J = 7.6 Hz, H₂), 7.46–7.33 (5H, m, H_{3,5,7,8,10}), 7.30–7.22 (2H, m, H_{4,9}), 7.09–6.99 (3H, m, H_{5;6,7}·), 6.97–6.81 (2H, m, H_{4;8}·); ¹³C NMR (125 MHz, DMSO- d_6) δ 198.59 (C_{28} , M-CO), 197.36 ($C_{27,29}$, 2M-CO), 163.72 (C_8), 159.53 (C_{17}), 148.11 (C_{20}), 147.43 (C_{10}), 143.58 (C_{16}), 141.41 (C_2), 138.20 (C_4), 131.80 (C_7), 129.67 ($C_{22,24,11}$), 129.49 ($C_{14,12}$), 129.39 (C_5), 129.10 (C_6), 126.26 (C_3), 124.29 (C_{13}), 122.25 (C_{23}), 120.48 (C_{15}), 117.74 ($C_{21,25}$); IR (KBr) v 3078 (=C–H)_{stretching} 2036, 1944, 1920 (Re–CO)_{stretching}, 1666 (C=O)_{stretching}, 1550 (C=N)_{stretching}, 1458 (C=C)_{ar. stretching}, 1249 (C–N)_{stretching} cm⁻¹; MS m/z (%): 645 (100) [M⁺], 647 [M⁺²].

$[(Re(CO)_3L^2)Cl] (C^2)$

Yield: 52.43% (52.43 mg) of tawny brown amorphous solid; m.p. >300 °C; mol. wt.: 678.50 g/mol $(C_{24}H_{13}Cl_2N_4O_4Re)$; ¹H NMR (400 MHz, DMSO- d_6) δ 12.77 (1H, s, H_{2}), 7.57 (1H, d, J = 7.2 Hz, H_{2}), 7.49 (1H, d, $J = 7.6 \text{ Hz}, H_5$, 7.40–7.37 (2H, m, $H_{3.4}$), 7.28 (1H, d, J = 7.2Hz, H₇), 7.26 (1H, d, J = 7.6 Hz, H₈), 7.20 (1H, s, H₁₀), 7.13–7.02 (3H, m, $H_{5,6,7}$), 6.99–6.87 (2H, m, $H_{4,8}$); ¹³C NMR (125 MHz, DMSO- d_6) δ 198.31 (C₂₈, M-CO), 197.21 $(C_{27,29}, 2M-CO), 163.09 (C_8), 161.12 (C_{17}), 152.55 (C_{20}),$ 148.16 ($C_{10,16}$), 145.43 (C_2), 138.18 (C_4), 131.19 (C_7), 129.51 (C₁₃), 129.04 (C_{22,24}), 128.82 (C₁₂), 127.21 (C₁₄), $126.79 (C_5)$, $126.59 (C_6)$, $125.48 (C_3)$, $124.43 (C_{11})$, 122.01 (C_{23}) , 120.48 (C_{15}) , 117.53 $(C_{21,25})$; IR (KBr) v 3062 (=C-H)_{stretching}, 2036, 1913, 1874 (Re-CO)_{stretching}, 1635 (C=O) stretching, 1550 (C=N)_{stretching}, 1450 (C=C)_{ar. stretching}, 1188 $(C-N)_{\text{stretching}}$, 694 $(C-Cl)_{\text{bending}}$ cm⁻¹; MS m/z (%): 679 (100) [M⁺], 681 [M⁺²], 683 [M⁺⁴].

$[(Re(CO)_3L^3)Cl] (C^3)$

Yield: 54.23% (54.23 mg) of red amorphous solid; m.p. >300 °C; mol. wt.: 678.50 g/mol ($C_{24}H_{13}Cl_2N_4O_4Re$); ¹H NMR (400 MHz, DMSO- d_6) δ 12.71 (1H, s, H₂·), 7.56 (1H, d, J = 7.2 Hz, H₂), 7.49–7.45 (2H, m, H_{7,5}), 7.46 (1H, d, J = 7.6 Hz, H₁₀), 7.34–7.17 (2H, m, H_{3,8}), 7.15–6.98 (2H, m, H_{4,9}), 6.95–6.89 (4H, m, H_{4,5,7,8}°); ¹³C NMR (125 MHz, DMSO- d_6) δ 198.66 (C_{28} , M-CO), 197.51 ($C_{27,29}$, 2M-CO), 164.80 (C_8), 160.58 (C_{17}), 150.75 (C_{10}), 147.13 (C_{20}), 145.31 (C_{16}), 141.66 (C_2), 137.17 (C_4), 133.49 (C_7), 131.17

 $(C_{22,24})$, 129.71 (C_{11}) , 128.98 $(C_{12,14})$, 127.45 (C_5) , 126.99 (C_{23}) , 125.92 (C_6) , 125.11 (C_3) , 123.81 (C_{13}) , 120.57 (C_{15}) , 118.19 $(C_{21,25})$; IR (KBr) v 3047 $(=C-H)_{\text{stretching}}$, 2036, 1944, 1920 $(\text{Re}-\text{CO})_{\text{stretching}}$, 1666 $(C=O)_{\text{stretching}}$, 1550 $(C=N)_{\text{stretching}}$, 1458 $(C=C)_{\text{ar. stretching}}$, 1242 $(C-N)_{\text{stretching}}$, 648 $(C-Cl)_{\text{bending}}$ cm⁻¹; MS m/z (%): 679 (100) $[M^+]$, 681 $[M^{+2}]$, 683 $[M^{+4}]$.

$[(Re(CO)_3L^4)Cl](C^4)$

Yield: 52.96% (52.96 mg) of bright red amorphous solid; m.p. >300 °C; mol. wt.: 712.94 g/mol $(C_{24}H_{12}Cl_3N_4O_4Re)$; ¹H NMR (400 MHz, DMSO- d_6) δ 12.70 (1H, s, H_2), 7.58 (1H, d, J = 7.6 Hz, H_2), 7.56–7.52 (3H, m, H_{5.7.8}), 7.45–7.39 (3H, m, H_{3,4,10}), 7.32–7.20 (2H, m, H_{5',7'}), 6.95-6.86 (2H, m, H_{3',8'}); ¹³C NMR (125 MHz, DMSO- d_6) δ 198.86 (C₂₈, M-CO), 197.34 (C_{27.29}, 2M-CO), $162.05 (C_8)$, $158.73 (C_{17})$, $148.13 (C_{20})$, $145.87 (C_2)$, 143.51 $(C_{10,16})$, 138.28 (C_4) , 133.85 (C_7) , 131.39 (C_{13}) , 130.62 $(C_{22,24})$, 129.20 (C_{12}) , 127.64 (C_{14}) , 127.04 (C_5) , 126.56 (C_{23}) , 126.09 (C_6) , 125.62 (C_3) , 124.77 (C_{11}) , 122.51 (C_{15}) , 117.89 ($C_{21,25}$); IR (KBr) v 3055 (=C-H)_{stretching}, 2036, 1944, 1890 (Re-CO)_{stretching}, 1658 (C=O)_{stretching}, 1550 (C=N)_{stretching}, 1450 (C=C)_{ar. stretching}, 1211 (C-N)_{stretching}, 686 (C–Cl)_{bending} cm⁻¹; MS *m/z* (%): 711 (100) [M⁺], 713 $[M^{+2}]$, 715 $[M^{+4}]$, 717 $[M^{+6}]$.

$[(Re(CO)_3L^5)Cl](C^5)$

Yield: 58.66% (58.66 mg) of orange amorphous solid; m.p. >300 °C; mol. wt.: 712.94 g/mol ($C_{24}H_{12}Cl_3N_4O_4Re$); ¹H NMR (400 MHz, DMSO- d_6) δ 13.08 (1H, s, H₂·), 7.80 $(1H, d, J = 7.2 Hz, H_2), 7.67 (1H, d, J = 7.6 Hz, H_7), 7.60$ (1H, d, J = 7.2 Hz, H₅), 7.49 (1H, d, J = 7.6 Hz H₁₀), 7.48 $(1H, s, H_{7})$, 7.31 $(1H, t, J = 7.6 Hz, H_3)$, 7.27–7.14 $(2H, m, H_{7})$ $H_{4.8}$), 7.09 (1H, t, J = 7.6 Hz, H_9), 7.03–6.92 (2H, m, $H_{4.5}$); ¹³C NMR (125 MHz, DMSO- d_6) δ 198.70 (C₂₈, M-CO), 197.32 (C_{27.29}, 2M-CO), 161.42 (C₈), 159.03 (C₁₇), 153.83 (C_{20}) , 148.09 (C_{10}) , 147.28 (C_{16}) , 141.76 (C_2) , 138.33 (C_4) , 133.76 (C_7), 131.98 (C_{22}), 130.58 (C_{11}), 129.14 ($C_{12.14}$), 128.55 (C₅), 127.48 (C₂₄), 126.84 (C₆), 126.14 (C₂₁), 125.85 (C_{23}) , 125.33 (C_3) , 124.24 (C_{13}) , 120.48 (C_{15}) , 119.51 (C_{25}) ; IR (KBr) v 3047 (=C-H)_{stretching}, 2028, 1920, 1882 (Re-CO)_{stretching}, 1643 (C=O)_{stretching}, 1550 (C=N)_{stretching}, 1450 (C=C)_{ar. stretching}, 1180 (C-N)_{stretching}, 640 (C-Cl)_{bend} $_{\text{ing}}$ cm⁻¹; MS m/z (%): 711 (100) [M⁺], 713 [M⁺²], 715 $[M^{+4}]$, 717 $[M^{+6}]$.

$[(Re(CO)_3L^6)Cl](C^6)$

Yield: 56.62% (56.62 mg) of carrot orange amorphous solid; m.p. >300 °C; mol. wt.: 747.38 g/mol ($C_{24}H_{11}Cl_4N_4O_4Re$); ¹H NMR (400 MHz, DMSO- d_6) δ 13.06 (1H, s, H₂·), 7.87 (1H, d, J=7.2 Hz, H₂), 7.69 (1H, d, J=7.6 Hz, H₅), 7.63 (1H, d, J=8.0 Hz, H₇), 7.61–7.53 (2H, m, H_{3,4}), 7.49 (1H, d, J=8.0 Hz, H₈), 7.48 (1H, s, H₅·), 7.35 (1H, s, H₁₀), 7.32 (1H, d, J=6.8 Hz, H₈·), 6.96 (1H, d, J=7.2 Hz, H₇·); ¹³C NMR (125 MHz, DMSO- d_6) δ 198.90 (C_{28} , M-CO), 197.13 ($C_{27.29}$, 2M-CO), 160.35 (C_{8}), 158.28

 $\begin{array}{l} (C_{17}),\ 148.15\ (C_{20}),\ 147.44\ (C_{10,16}),\ 143.09\ (C_{2}),\ 139.31\\ (C_{4}),\ 138.25\ (C_{7}),\ 136.92\ (C_{22}),\ 133.77\ (C_{13}),\ 132.90\ (C_{12}),\\ 132.14\ (C_{14}),\ 132.04\ (C_{5}),\ 131.91\ (C_{24}),\ 131.85\ (C_{6}),\ 129.18\\ (C_{21}),\ 126.07\ (C_{23}),\ 124.85\ (C_{3}),\ 124.06\ (C_{11}),\ 122.39\ (C_{15}),\\ 118.03\ (C_{25});\ IR\ (KBr)\ v\ 3031\ (=C-H)_{stretching},\ 2036,\ 1974,\\ 1882\ (Re-CO)_{stretching},\ 1643\ (C=O)_{stretching},\ 1550\ (C=N)_{stretching},\ 1458\ (C=C)_{ar.\ stretching},\ 1180\ (C-N)_{stretching},\ 640\ (C-Cl)_{bending}\ cm^{-1};\ MS\ m/z\ (\%):\ 746\ (100)\ [M^+]. \end{array}$

2. 4. Computational Study

2. 4. 1. DFT Study

The optimal structural geometry of Re(I) complexes based on tryptanthrin was calculated using the DFT/ B3LYP approach with different base sets in Gaussian 09 software.²⁵ The molecular visualization tool Gauss View is used to display the Gaussian files. Quantum chemical parameters are estimated from the HOMO-LUMO energies based on the numerical pattern shown in the gas-phase view of the compounds. The optimized structures provided information on important bond lengths, excitation energies, and effective charges of coordinating groups. Frontier molecular orbitals (FMOs) energy gap of the ligand and its metal complexes calculated to determine electronic properties related to dynamic stability and chemical reactivity.²⁶ In the Schiff base ligand, the π – π * electron transfer was facilitated by the HOMO and LUMO orbitals, which were mostly located on the donor site of the ligand. In the L-M complex, these orbitals are found around the metal center.27

2. 4. 2. Molecular Docking Study

The process of molecular docking involves the creation of an optimal conformation for a protein and a drug, with their relative orientations optimized to minimize the free energy of the entire system. This process aims to replicate the molecular recognition process that occurs in biological systems.²⁸ In order to perform this process, various parameters such as interaction mode, connectivity, and connection energy are calculated using software tools such as Auto Dock. In this study, the Auto Dock-1.5.6 program was used in conjunction with DNA and BSA macromolecules to carry out molecular docking investigations on the ligand and rhenium metal complexes. The crystal structures of DNA and BSA were obtained from the Protein Data Bank, a global resource for processing and sharing 3D biological macromolecular structure data. Water molecules were eliminated from the DNA/BSA structures, and the Kollman charges and necessary hydrogen atoms were added to the receptor structure. To study the bonding condition, DNA was examined in a cube box with dimensions of $62 \times 72 \times 114 \text{ Å}^3$ and $112 \times 31 \times 33 \text{ Å}^3$. PDB files for each compound and DNA/BSA translated into PDBQT format using AutoDockTools-1.5.6. The command prompt used Auto Dock Vina to conduct a docking investigation between the substances and DNA/BSA.^{29,30} It required one run and produced output files that will be viewed using PyMOL. All compounds with DNA/BSA docked structures were stored in PDB format for further analysis. In summary, molecular docking was used to investigate the interaction between ligands and rhenium metal complexes with DNA and BSA macromolecules. This involved a detailed process of preparing the receptor structures and running the docking simulations using Auto Dock software. The results of this study provide insights into the potential binding modes and energies of these compounds with DNA and BSA, which could have important implications for drug design and development.

2. 4. 3. ADME Study

The field of medicinal chemistry is rapidly expanding, but the development of a new medication is a complex and expensive process that can take more than a decade and costs billions of dollars. With thousands or even millions of compounds to consider, only a small fraction will meet the rigorous requirements necessary to become an approved medication. In order to increase the efficiency and success of drug development, assessments such as ADMET properties are used to predict the likelihood of a compound's success.³¹ These assessments focus on the five processes: absorption, distribution, metabolism, excretion, and toxicity (ADMET) to determine how a chemical substance will behave inside the human body. By evaluating a substance's physicochemical properties, ADMET assessments can help identify compounds that are more likely to succeed in clinical trials. The Swiss ADME web server is a valuable tool in this process, as it provides free calculations of physicochemical parameters based on a substance's structure.

2. 5. Biological Study

2. 5. 1. Binding of the DNA Study by Absorption Titration

A popular technique for studying the nucleic acids with nucleic acid interaction of ligands or metal compounds is UV-VIS spectroscopy. The UV-VIS absorbance spectra and DNA-mediated hypochromism of ligands or metal compounds is determined in a series to evaluate metal complex binding to CT-DNA. By calculating the absorbance at 260–280 nm and evaluating ϵ_a of 6600 $M^{-1} \mbox{cm}^{-1}$ the concentration of the calf thymus DNA will be ascertained. CT-DNA and the method outlined in the pertinent literature are both employed to assess the interaction of binding synthesized ligands with Re(I) metal compounds. 32

2. 5. 2. Viscosity Measurement

The binding mechanism of the synthesised compounds with calf thymus DNA was assessed using a viscos-

ity measuring method. The viscosity of the DNA solution increases as molecules intercalate between DNA base pairs.³³ On other hand, when compounds bind to the grooves of DNA, the viscosity increases due to the reduction in the double helix length of DNA. A trend for increasing viscosity can distinguish the intercalation-binding mode from the groove-binding mode. In this study, metal complexes showed a higher increase in viscosity compared to the corresponding ligands, indicating stronger binding of the metal complexes to the ligands.³⁴

2. 5. 3. Fluorescence Quenching Analysis by DNA Binding

A fluorescence spectrometer is a highly precise, quick, and sensitive tool for analyzing DNA binding activity even at very low concentrations of compounds and DNA. This study uses the fluoromax-4, HORIBA spectrofluorometer to perform fluorescence-quenching analysis, which provides relevant results related to the binding capacity of the synthetic chemicals within DNA. The studies focuses on explaining how chemicals bind with DNA *via* the intercalation, with traditional intercalating agent EtBr used as a fluorescence marker.^{35,36}

2. 5. 4. BSA Binding Study by Absorption Spectra

The protein BSA is essential for the movement of both endogenous and foreign materials in plasma. Plasma, though, can be bad for our molecules. Two important things occur when our molecules bind to BSA in the plasma: (1) the toxicity of the drug is decreased, and (2) the bioavailability of the chemical is raised.³⁷ The absorption spectra of proteins change when our compounds, referred to as quenchers, engage with BSA.³⁸ This alteration provides information about the binding affinities and modes of all synthetic compounds toward BSA. By understanding this interaction, we can design and develop effective and safe anticancer drugs.³⁹

2. 5. 5. Fluorescence Quenching Analysis by BSA Binding

Tryptophan, phenylalanine, and tyrosine are only a few of the particular amino acid residues that give BSA its luminous features. BSA is a good fluorescent marker for analyzing conformational changes brought on by drug interactions thanks to these residues. Tryptophan has the highest fluorescence intensity of these residues and is crucial in suppressing the fluorescence of BSA. Trp-213 and Trp-134, both residues of the tryptophan found in the BSA, are respectively placed on the surface and within the hydrophobic pocket of the molecule. A total 100 μ L of BSA and 2400 μ L of phosphate buffer were used for the protein binding experiment. The experiment comprised employing varying quantities of ligands L^1-L^6

and complexes C^1 – C^6 in a room temperature environment (0, 10, 20, 30, 40, and 50 μ L). Utilizing a spectro-fluorometer with a 4.5 nm slit width and covering the wavelength range of 280–550 nm, emission spectra were captured. For BSA, 280 nm was chosen as the excitation wavelength.

2. 5. 6. Antibacterial Activity

Broth dilution method was used to evaluate the antibacterial properties of the synthesized compounds. Antibacterial properties of these compounds were tested against two Gram positive bacterial strains, namely Staphvlococcus aureus (MTCC 7193), and Bacillus subtilis (MTCC 3160) and three Gram negative bacterial strains: Escherichia Coli (MTCC 433), Serratia marcescens (MTCC 7103), and Pseudomonas aeruginosa (MTCC P09). An established and standardized approach for assessing a compound's antibacterial activity is the broth dilution method. 41,42 In this procedure, test compounds are serially diluted in a liquid growth medium. 43,44 The effectiveness of a drug in suppressing bacterial growth can be evaluated by measuring the MIC (minimum inhibitory concentration).45 This method is useful in evaluating the efficacy of antimicrobial compounds against different bacterial strains and in comparing the relative effectiveness of different compounds.46

2. 5. 7. Brine Shrimp Lethality Bioassay (BSLB)

To study cytotoxicity for the produced compounds, the most significant BSLB was used as reported by R. A. Dabhi *et al.* (2022).⁴⁷ The cytotoxicity assay employed in the study is cost-effective and requires less time compared to other assays, making it advantageous for determining the cytotoxicity of drugs. In accordance with the protocol, the assay involved the preparation of a saline water (2.5%) solution for hatching of *Artemia cysts* type eggs.⁴⁸ Further nauplii (10) were added to the test-tube already containing the brine water (5 mL) and additionally freshly made saline water (5 mL) for the assay. The percentage of *Artemia cyst* mortality was seen to grow in step with the increase in chemical concentration (2, 4, 8, 12, 16, and 20 μ M).⁴⁹ The resulting graph showed a linear relationship, making it possible to calculate the compounds' LC₅₀ values.

2. 5. 8. Anticancer Activity

Cancer patients benefit greatly from chemotherapy, and the IC_{50} values of synthesised compounds are used to evaluate their efficacy as chemotherapeutic agents.⁵⁰ To determine whether a substance has the potential to be used in the treatment of cancer, its capacity to suppress cell proliferation must be evaluated.^{51,52} The cytotoxicity *in vit-ro* experiment was performed on the breast cancer cell line MCF-7 to assess their anticancer effectiveness.⁵³

3. Result and Discussion

3. 1. NMR, IR, Mass, Conductivity Measurements, and Electronic Spectra

It was found that the ligands' aromatic protons resonate between δ 6.85 to 8.54 ppm. The ligands' NH proton signals are visible in the δ 12.77 to 13.49 ppm range. The NH proton signal, notably in the range from δ 12.70 to 13.08 ppm, were shifted into the up-field region in the organometallic complexes. The presence of an aromatic environment is indicated by signals in the range of δ 110–170 ppm that are found in the ¹³C NMR data for ligands L¹-L⁶ and complexes C¹-C⁶. In Re(CO)₅Cl crystal structure the four CO ligands are positioned equatorially, while one CO ligand is positioned axially which is exactly opposite to the Cl atom. 46,54 Re(I) complexes are formed when the heterocyclic bidentate ligand approaches from the equatorial position and then displaces two CO ligands. 55,56 The 13C NMR spectra show that the facial arrangement has two different low-field signals in the regions of δ 195–199 and 196–198 ppm, respectively, which reflect the configuration of the CO ligands in the Re(I) complexes. The facial isomer is responsible for the biological activity.⁵⁷ It has a high distribution and polarity as compared to the meridional isomer.⁵⁸

IR spectroscopy was used to further comprehend the Re(I) complexes' characteristics. The stretching bands seen in the spectra, which ranged from 1735–2021 cm⁻¹, confirm the presence of three coordinated carbonyl ligands. This indicates that they are present in the rhenium metal complexes. It is interesting to note that the stretching frequencies of the CO group in complexes are lower than the stretching frequencies of free CO (2143 cm⁻¹). This result is explained by the back-bonding phenomena, in which electrons are given from the metal \rightarrow CO π back donation into the π^* CO orbital. The total bond strength of CO in the complexes decreases because of this interaction, which also increases the Re–CO bonds.

The mass spectra and fragmentation pattern of the ligands based on tryptanthrin are included in the electronic supplementary information. The molecular ion peak [M]⁺ is represented by the m/z 372.0 peak, while the appearance of the m/z 374.0 and [M + 2]⁺ peaks are due to the chlorine substitution in the ligand L^2 , respectively. The molecular ion peak [M]⁺ for the ligand L^6 is found at m/z 440.0. Additionally, separate peaks with intensities of 0.9:1:0.3:0.1 are found at [M + 2]⁺ m/z 442.0, [M + 4]⁺ m/z 446.0, and m/z [M + 6]⁺ 452.0, respectively. Three chlorine substitutions are involved, according to these peaks. All synthesized compounds' ¹H, ¹³C NMR, mass, and IR spectra are shown in the electronic supplementary information (ESI 1).

Conductance was used to examine the ionic and electrolytic characteristics of synthesized compounds. At a temperature of 30 \pm 5 °C, the complexes' conductance was measured in DMSO solutions. The complexes demonstrate a non-ionic and non-electrolytic character, as evidenced by the conductance values (10.5–18.2 Ω^{-1} cm² mol $^{-1}$). A $\mu_{\rm eff.}$ value zero B. M. indicates that all of the complexes are diamagnetic and have the low spin configuration d 6 (t $_2$ g 6 eg 0). Electronic spectra of the complexes taken in DMSO solution reveal a band in the 250–270 nm region that corresponds to the $\pi-\pi^*$ transition and a peak in the 300–400 nm region that denotes the MLCT. These results support the hypothesis that the Re(I) metal complexes have a distorted octahedral geometry.

3. 2. DFT Theory

The electron density cloud revealed by surface-mapped charges is consistent with the results of biomolecular docking, which suggests that the most electronegative components form hydrogen bonds with biomolecules and can be used to determine the binding sites. In order to understand biological processes requiring an electron transport channel, the HOMO-LUMO energy difference is essential. Tran-

Table 1. Summary of the HOMO-LUMO	energy	differences	and	docking	energy	of ligand	and	tryptan-
thrin-based Re(I) complexes.								

	DF	Γ Study		D	ocking Energ	S y
Compounds	HOMO (eV)	LUMO (eV)	HOMO-LUMO energy differences	DNA kcal/mol)	BSA kcal/mol)	TOPO II kcal/mol)
$\overline{L^1}$	6.0276	3.4060	2.6215	-8.3	-9.9	-11.8
L^2	6.1928	3.5168	2.6760	-8.6	-10.4	-10.7
L^3	6.1724	3.5035	2.6689	-8.5	-9.6	-11.9
L^4	6.3294	3.6107	2.7187	-9.2	-9.6	-11.6
L^5	6.3106	3.4583	2.8523	-8.5	-10.6	-12.6
L^6	6.4744	3.5688	2.9056	-8.7	-9.8	-12.1
C^1	5.6352	3.9559	1.6793	-8.1	-9.9	-9.7
\mathbb{C}^2	5.7582	4.1053	1.6529	-8.5	-9.1	-10.0
\mathbb{C}^3	5.7633	4.0759	1.6874	-8.2	-8.9	-10.0
C^4	5.8817	4.2332	1.6485	-8.6	-10.1	-9.7
C^5	5.8561	4.2109	1.6452	-8.0	-8.9	-9.9
C^6	5.9704	4.3600	1.6104	-7.9	-9.6	-10.2

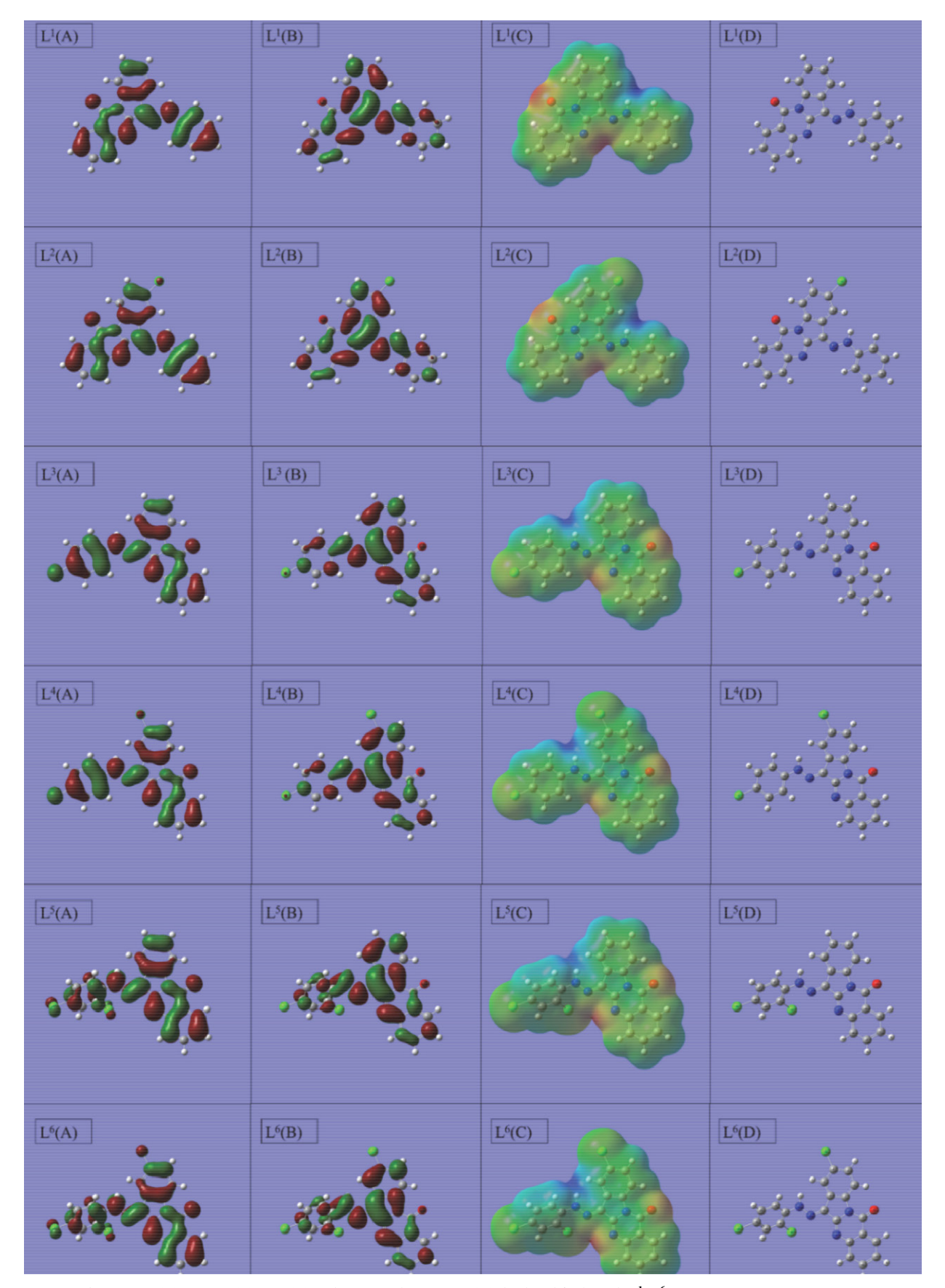
sition metal complexes' kinetic stability, chemical reactivity, and biological activity are all predicted using the energy difference between the HOMO–LUMO orbitals (Table 1). The energy gaps for complexes C^1 – C^6 are 1.6793, 1.6529, 1.6874, 1.6485, 1.6452, and 1.6104 eV, respectively (Figures 2 and 3). A smaller energy gap promotes smoother electron transport, which is important for bioactivity through electron transfer. Compound C_6 has the smallest energy gap and exhibits strong antibacterial and anticancer properties. In Table 2, the Mulliken charges of quinoxaline-based Re(I) complexes C^1 – C^6 and ligands L^1 – L^6 are summarised (the most positive and the most negative five atom charges). The bond length, bond angle, and Mulliken charges for ligands L^1 – L^6 and complexes C^1 – C^6 are shown in electronic supplementary information (ESI 2).

3. 3. Docking Study

The goal of computational docking research using the widely-used software program AutoDock Vina is to forecast the preferred binding mode and interaction locations of small molecules or ligands with target macromolecules like proteins or nucleic acids.⁵⁴ In order to determine binding energy of possible receptor-like ligands and compounds, this program combines molecular mechanics with empirical scoring functions. Based on this energy evaluation, it predicts the most stable conformation. Studies have shown that the binding energies of ligands L^1-L^6 with DNA, as predicted by AutoDock Vina, typically fall in the range between -8.3 to -9.2 kcal/mol. This range of values indicates a strong binding affinity between the ligands and DNA, which is desirable for potential drug candidates. Similarly, Re(I) complexes C^1 - C^6 have also been studied using AutoDock Vina, and their binding energies with DNA all fall within the range of -7.9 to -8.6 kcal/mol. Although binding energies for Re(I) complexes with DNA are slightly lower than those of ligands, they still indicate a strong binding affinity, which could be useful in applications such as imaging or therapeutics. In the context of computational docking studies, a negative binding energy

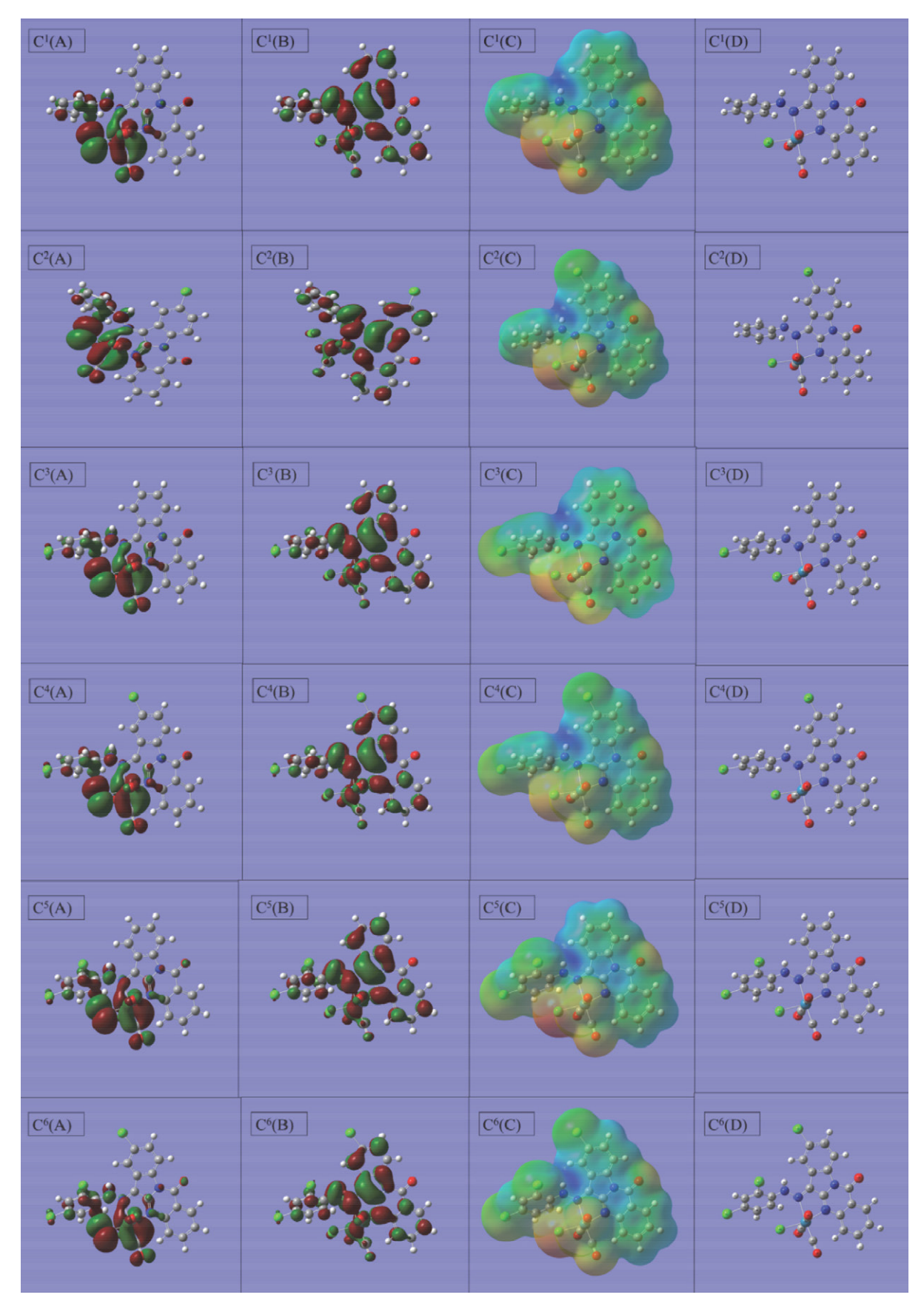
Table 2. Mulliken charges of ligands L^1-L^6 and rhenium(I) metal complexes C^1-C^6 .

	Most negative charge	Most positive charge		Most negative charge	Most positive charge
$\overline{L^1}$	24N (-0.35335)	13N (0.07782)	C ¹	4C (-0.36207)	12C (0.12663)
	27C (-0.32411)	14C (0.14410)		1C (-0.31561)	2C (0.20970)
	30C (-0.31968)	3C (0.16510)		13N (-0.30104)	3C (0.27875)
	5C (-0.29061)	2C (0.22322)		23N (-0.29971)	37Re (0.28489)
	1C (-0.28117)	26C (0.29198)		27C (-0.28049)	38Cl (0.28758)
$\overline{L^2}$	23N (-0.35247)	12N (0.07935)	\mathbb{C}^2	1C (-0.30591)	11C (0.13612)
	26C (-0.32197)	13C (0.14476)		4C (-0.30586)	2C (0.209034)
	29C (-0.31943)	3C (0.18246)		12N (-0.30256)	37Cl (0.23384)
	1C (-0.26943)	2C (0.21980)		22N (-0.29183)	36Re (0.29485)
	10N (-0.26317)	25C (0.29264)		26C (-0.28169)	3C (0.29771)
L^3	23N (-0.35163)	12N (0.07844)	C ³	4C (-0.35620)	11C (0.13945)
	29C (-0.31503)	13C (0.14441)		1C (-0.31318)	36Cl (0.16812)
	26C (-0.30206)	3C (0.16518)		12N (-0.30220)	2C (0.21322)
	5C (-0.29016)	2C (0.22402)		22N (-0.27595)	3C (0.27825)
	1C (-0.28042)	25C (0.29738)		23N (-0.27324)	35Re (0.30050)
$\overline{L^4}$	23N (-0.35083)	12N (0.07995)	C ⁴	12N (-0.30723)	11C (0.14675)
	29C (-0.31482)	13C (0.14509)		1C (-0.30386)	25C (0.15633)
	26C (-0.29992)	3C (0.18256)		4C (-0.30263)	2C (0.21277)
	1C (-0.26893)	2C (0.220697)		23N (-0.28844)	3C (0.29942)
	10N (-0.26290)	25C (0.29791)		22N (-0.28706)	35Re (0.30789)
L ⁵	23N (-0.34009)	12N (0.07801)	C ⁵	4C (-0.35094)	37C (0.10036)
	5C (-0.29133)	13C (0.14346)		12N (-0.31432)	11C (0.14383)
	26C (-0.28880)	3C (0.16764)		1C (-0.31239)	2C (0.21318)
	1C (-0.28240)	2C (0.22197)		22N (-0.30076)	3C (0.28067)
	10N (-0.26667)	25C (0.40708)		23N (-0.28999)	34Re (0.31642)
L ⁶	23N (-0.33941)	12N (0.07948)	C ⁶	12N (-0.31386)	11C (0.14926)
	26C (-0.28670)	13C (0.14414)		1C (-0.30514)	2C (0.21142)
	1C (-0.27076)	3C (0.18446)		4C (-0.30112)	34Re (0.30523)
	10N (-0.26241)	2C (0.21886)		22N (-0.29900)	3C (0.30545)
	29C (-0.25226)	25C (0.40823)		23N (-0.28821)	25C (0.32456)



 $\textbf{Figure 2}. \ \ \text{The HOMO (A), LUMO (B), ESP (C) and optimized structures (D) displayed for ligands } \\ L^1-L^6.$

Padariya et al.: Synthesis, Characterization and Biological Applications of $\ \dots$



 $\textbf{Figure 3}. \ \ \text{The HOMO (A), LUMO (B), ESP (C) and optimized structures (D) \ displayed for \ rhenium (I) \ metal \ complexes \ C^1-C^6.$

Padariya et al.: Synthesis, Characterization and Biological Applications of $\ \dots$

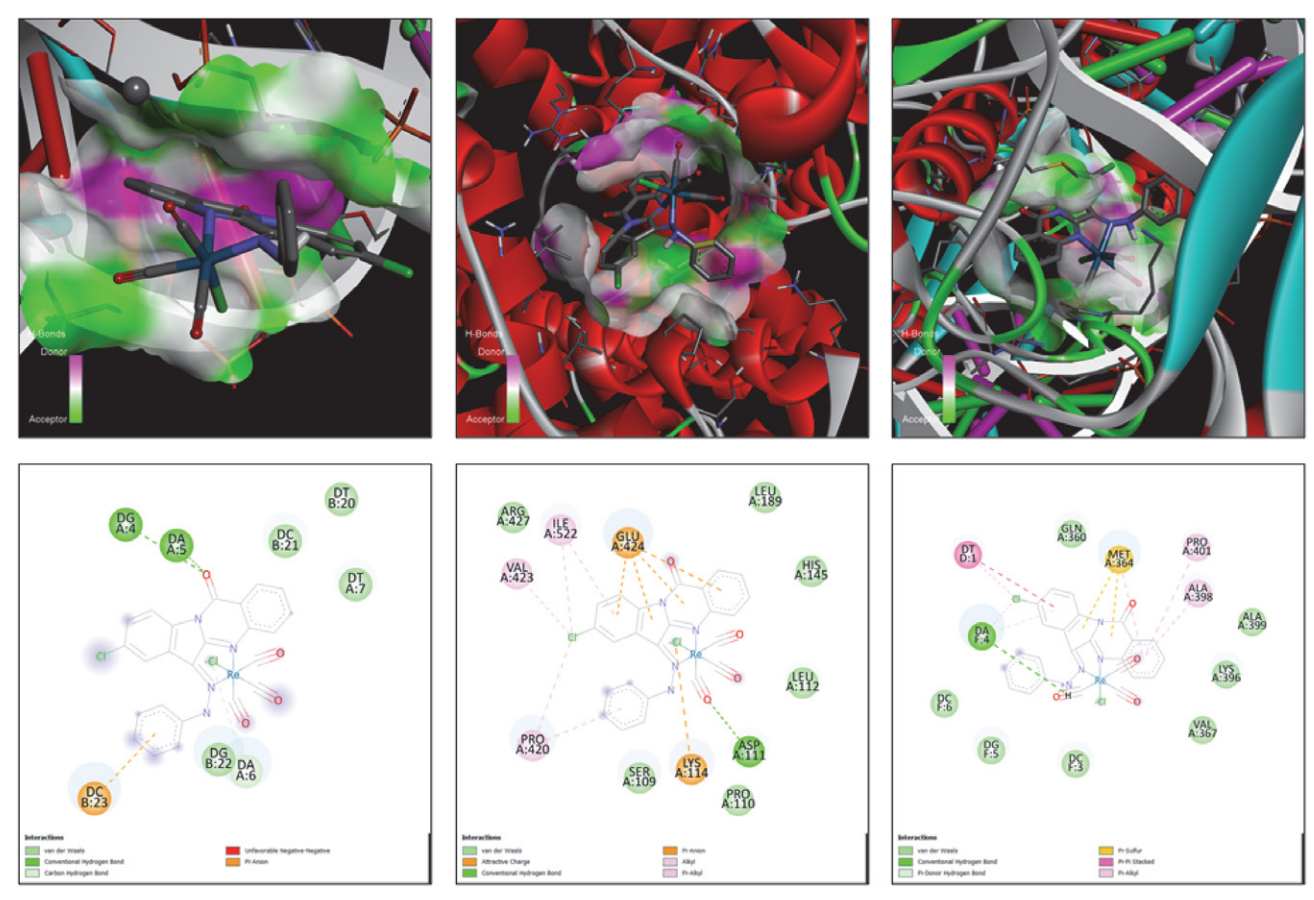


Figure 4. DNA, BSA, and TOPO II binding pose of the complex C^2 .

indicates the most favourable interaction between a small molecule or ligand and a macromolecule such as a protein or nucleic acid. This negative value represents the energy released or gained during the formation of the ligand–macromolecule complex and is an essential factor for determining stability and affinity of the compounds.

Complex C⁶ has very low binding energy of all the compounds examined, -7.9 kcal/mol, showing a better affinity for binding DNA than the other compounds. Table 1 displays the binding energy information for all synthesized compounds. Using a Discovery studio visualizer, the results of the docking research used to determine. Figure 4 displays the docked structure of complex C² with DNA, BSA, and TOPO II. Docking images for each of the synthesized compounds are displayed in the electronic supplementary information (ESI 3).

3. 4. ADME Study

Numerous parameters are provided by Swiss ADME, such as the number of H-bond acceptors, donors and specific atom counts, and molecular refractivity. The partition coefficient between water and n-octanol (log $P_{\text{o/w}}$), the topological polar surface area (TPSA), blood-brain barrier permeability (BBB), and bioavailability score.⁵⁵ On the basis of their examination of the physicochemical character-

istics of 2245 drugs in the World Drug Index (WDI) dataset that were authorized for clinical studies in phase II, Lipinski *et al.* proposed a set of five rules in 1997, emphasizing the significance of physicochemical and drug-likeness properties in drug design. Frysa value of 59.28 Å² for the ligands L¹–L⁶ indicates a comparatively small polar surface area, smaller than for carboplatin and larger than cisplatin. The ligands L¹–L⁶ have too much smaller values than topotecan, so, this indicates better activities than topotecan. The ligands L¹–L⁶ have higher molar refractivity values than cisplatin and carboplatin, and lower than topotecan, therefore showing higher activity than topotecan. Fr,58

All the ligands have strong permeability and bioavailability because these values are also below 140 $\mbox{Å}^2$. In other words, these substances are most favourable to be capable to pass via biological membranes with ease and have a higher potential of being absorbed into the blood-stream, suggesting favourable traits for their potential as therapeutic candidates.

The log $P_{\rm o/w}$ values, which measure lipophilicity, range between 2.89 and 3.76 for all the ligands. All of the ligands meet the range of values for lipophilicity that is generally accepted because these values are less than 5.

Quantitative classes of solubility in water are defined as insoluble (< -10), poorly (-10 to -6), moderately (-6 to

Ligands	L^1	L^2	L^3	L^4	L^5	L^6	Cisplatin	Carboplatin	Topotecan
Molecular weight	338.37	372.81	372.81	407.25	407.25	441.70	300.05	371.25	457.90
H-Bond acceptors	3	3	3	3	3	3	2	6	7
H-Bond donors	1	1	1	1	1	1	2	2	2
TPSA (Å ²)	59.28	59.28	59.28	59.28	59.3	59.3	6.48	59.08	104.89
$\log P_{ m o/w}$	2.89	2.97	3.15	3.38	3.53	3.76	_	-0.63	1.85
Molar Refractivity	102.86	107.87	107.87	112.88	113	118	21.16	38.49	114.81
log S	-5.08	-5.67	-5.67	-6.25	-6.25	-6.84	-0.826	-1.657	-3.02
Rotatable bonds	2	2	2	2	2	2	0	0	2
Lypinski's rule	0	0	0	0	1	1	_	0	0

Table 3. ADME properties of the synthesized compounds.

−4), soluble (−4 to −2), very (−2 to 0), and highly soluble (>0). ⁵⁵ According to the obtained results, ligand L¹ demonstrated a solubility rating as "moderately soluble" with a value of −5.1. The solubility ratings for the other ligands, which ranged from −5.1 to −6.8, were within the "soluble" range. It was discovered that there were 3 hydrogen bond donors and one hydrogen bond acceptor in each of the ligands. All of the developed derivatives were found to have molecular weights around 400, suggesting that they could move, diffuse, and absorb easily (Table 3). Good oral bioavailability is influenced by the rotatable bonds and it is essential that this number be lower than 10. There are two rotatable bonds in each of the ligands.

3. 5. UV-visible Absorption Titration Experiment

3. 5. 1. DNA Binding

The efficacy of a target molecule in treating a disease is partially dependent on its ability to bind tightly to DNA. Fortunately, anticancer drugs are designed to target DNA, which can be broken down in multiple ways, including through interactions with specific drug molecules. Moreover, cancer cells typically experience DNA damage first, which can potentially halt cell division and induce cell death.⁵⁹

The literature describes a technique using CT-DNA to evaluate the binding interaction of synthetic compounds. This technique involves using UV-visible spectroscopy experiments to study how tiny medicinal molecules interact with DNA.⁶⁰ The resulting UV-visible binding spectra of the compound intercalating in DNA show hypochromicity and bathochromic changes due to the stacking engagement of the ligand to DNA base pairs and aromatic chromophore.⁵² The compound's absorption bands display clear hypochromism at 380 nm with a small redshift as the amount of CT-DNA is increased, confirming an intercalation pattern that involves a stacking contact between the quinazoline ring and DNA base pairs.⁶¹

Tryptanthrin-based ligands L^1-L^6 and the related rhenium(I) complexes C^1-C^6 were studied for their binding mechanisms. The bathochromic and hypochromic shifts noticed, suggest that intercalation, a non-covalent

contact, was involved in the binding process. The complexes' binding constants (K_b) ranged from 0.98·10⁵ to $1.77 \cdot 10^5 \text{ M}^{-1}$, whereas the ligands' binding constants (K_b) ranged from $0.8 \cdot 10^5$ to $1.33 \cdot 10^5$ M⁻¹. Examining how the compounds interacted with DNA, it was discovered that adding a DNA solution caused clear spectroscopic changes. The spectra shifted by 3-5 nm as a result of these modifications which included hypochromism and bathochromic effect. The sequence of strength in which the ligands L^1-L^6 and complexes C^1-C^6 attach to CT-DNA was: C^6 > $C^4 > C^5 > C^2 > C^3 > C^1 > L^6 > L^4 > L^5 > L^2 > L^3 > L^1$. Equation $\Delta G = -RT \ln K_h$ was used to evaluate the Gibbs free energy (ΔG) at 298 K. Negative ΔG values showed that the compounds and DNA adduct formation were spontaneous. All complexes C¹-C⁶ displayed (Figures 5A and B) higher binding constant than the corresponding ligand, which is similar to previously reported Re(I) complexes.⁶²

3. 5. 2. Viscosity

The physical characteristics of the interaction can be investigated in order to identify the sort of binding that occurs between DNA and metal complexes. Increased solution viscosity indicates the intercalation-type binding, while decreased solution viscosity suggests the groove binding. Ethidium bromide is commonly used as an intercalator. When synthesized compounds interact with DNA, DNA solutions viscosity changes. Then flow time increases with each addition of the metal complex solution (Figures 5C and D). This demonstrates an interactive mode of binding, as confirmed by related research findings.⁶³

3. 5. 3. BSA Binding

It is essential to look into how medication molecules interact with blood plasma proteins in order to assure the targeted distribution of those molecules. Given that HSA (human serum albumin) and BSA (bovine serum albumin) share 78% of their structural similarities, BSA is randomly used as a reference group of amino acids in this research. Here, the binding constant value of ligands L¹–L⁶ is obtained in the range of 0.9–1.4·10⁴ M⁻¹, and in the case of complexes C¹–C⁶ is obtained in the range of 1.43–1.86·10⁴

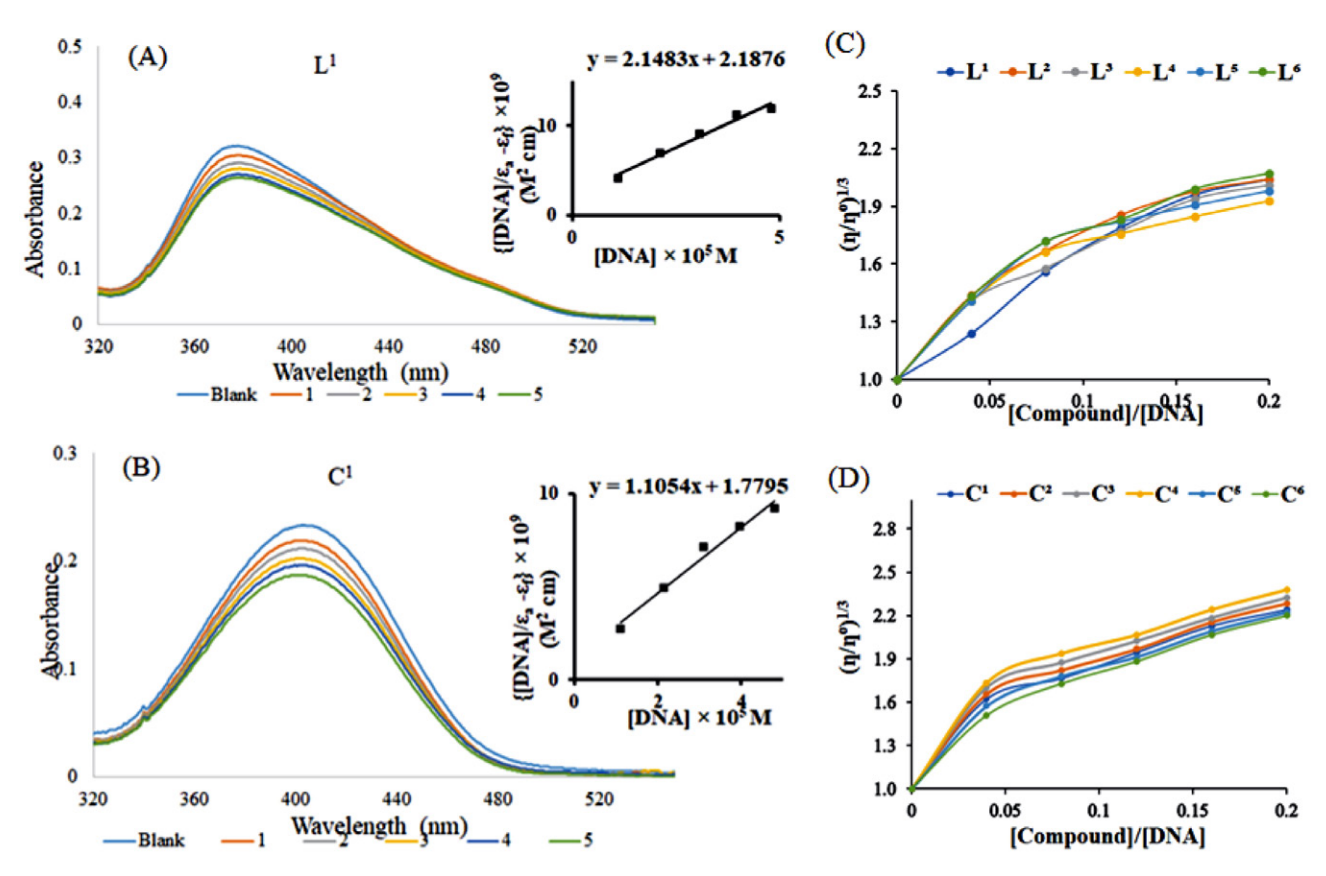


Figure 5. (A) and (B) The K_b value graph and DNA binding spectra of L^1 and C^1 . Viscosity (C) of ligands $L^1 - L^6$ and (D) of complexes $C^1 - C^6$.

 M^{-1} . For both BSA and DNA interaction, the complexes' C^1 – C^6 binding constants exhibit a consistent pattern. Figure 6 displays a typical spectrum for the BSA binding. The results of the docking investigation also show that the interaction of the substance with BSA has an almost the same pattern in the energy for binding, corroborating the exact binding predicted by theoretical binding predictions.

3. 6. Fluorescence Titration

3. 6. 1. Fluorescence Quenching Studies with DNA

The most efficient and sensitive method for analyzing the interaction between CT-DNA, EtBr (ethidium bromide), and compounds is the use of fluorescence methods. 65 EtBr one of the most delicate fluorescent probes, has a flat shape that intercalates with DNA to bind to it. It is frequently used to investigate DNA structural changes brought on by interactions with proteins or tiny chemicals. When present in an aqueous environment, EtBr typically exhibits modest fluorescence efficiency; however, the presence of DNA significantly increases its fluorescence intensity. Upon excitation at 520 nm, the CT-DNA-EtBr system exhibited a peak emission at 602 nm, indicating the presence of a maximum emission wavelength. As the concentration of the compound increases, the fluorescence intensity of the CT-DNA-EtBr system diminishes, while the wavelength of the emission maximum remains relatively unchanged; there are three possible explanations. Firstly, it

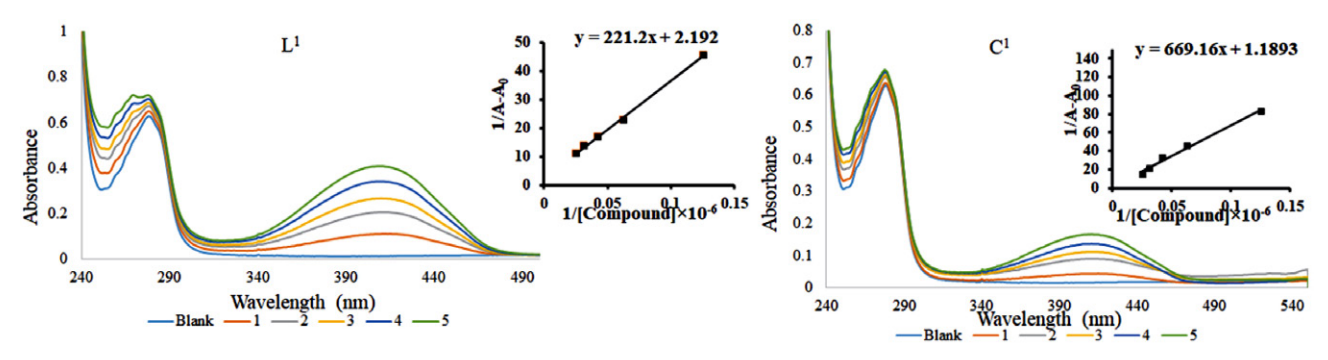


Figure 6. BSA binding spectra, and K_b value graph of L^1 and C^1 .

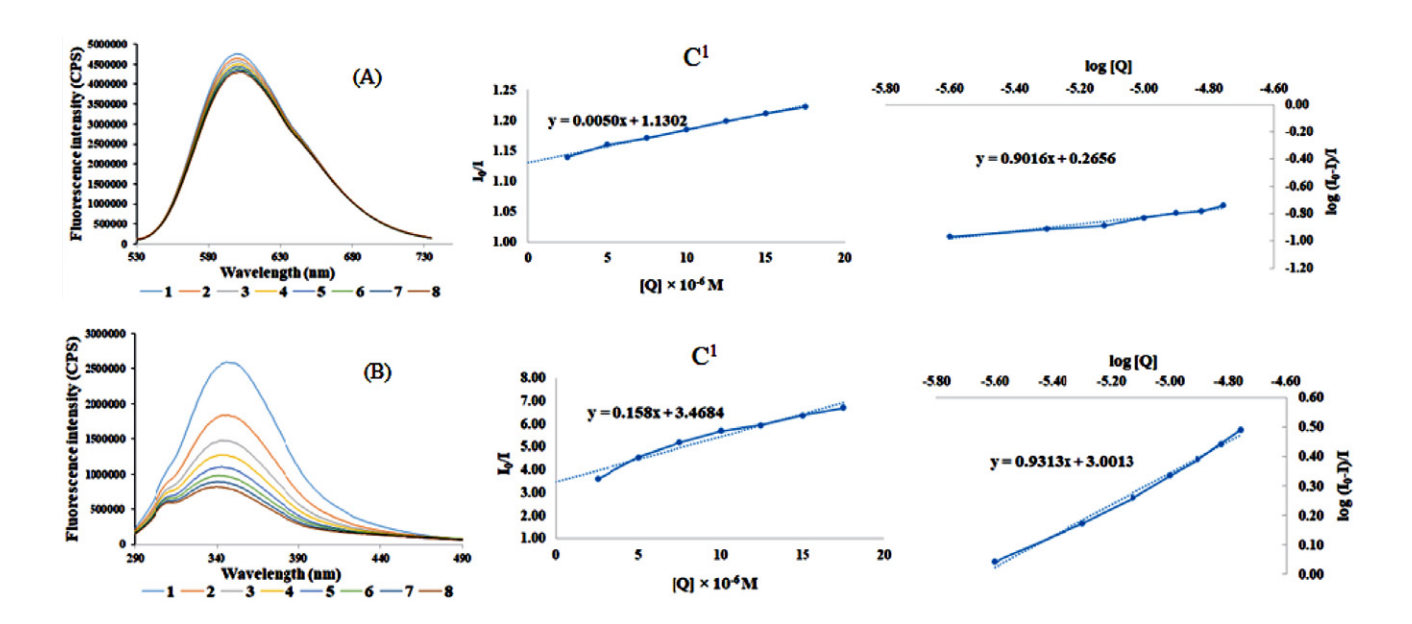


Figure 7. The fluorescence quenching spectra of DNA (A) and BSA (B), I_0/I versus [Q] and $\log I_0 - I/I$ versus [Q] plot for complex \mathbb{C}^1 .

could be due to the binding of compounds with EtBr, leading to fluorescence quenching. Secondly, the compounds might compete with EtBr for binding sites on the CT-DNA, thereby displacing intercalated EtBr from the complex and reducing the concentration for EtBr bound to CT-DNA (Figure 7A). Finally, it is possible that a new complex comprising compounds CT-DNA and EtBr will have formed as a result of the interaction between compounds and CT-DNA-EtBr. While the complexes C^1-C^6 displayed K_{sv} ranging in between 0.50 to 0.68·10⁴ M⁻¹, the ligands L^1-L^6 displayed values between 0.35 to 0.54·10⁴ M⁻¹.

3. 6. 2. Fluorescence Quenching Study with BSA

Proteins are vital macromolecules widely distributed in cells and essential for maintaining biological processes. Bovine serum albumin (BSA) is a large part of plasma protein and is essential for the body's transportation and metabolization of a variety of substances. ⁶⁶ This study aims to better understand how the target protein molecule, BSA, interacts with its environment. BSA was chosen because of its crucial attributes for medicine, exceptional binding capabilities, ease of accessibility, and structural resemblance to human serum albumin (HSA). ^{67,68} The complexes C¹–C⁴ Stern–Volmer binding constant ($K_{\rm sv}$) ranged from 1.58 to 1.95·10⁴ M⁻¹, while the ligands L¹–L⁴ showed values between 0.85 to 0.149·10⁴ M⁻¹. The representative fluorescence spectra, I_0/I plot, and log I_0 –I/I vs. log [Q] graph for complex C¹ is shown in Figure 7B.

3. 7. Anticancer Activity

In the MCF-7 cell line, we used a colorimetric technique to evaluate the compounds anticancer potential.

Cell viability was variable and increased with sample concentration for both the tryptanthrin-based ligand and Re(I) complexes.⁶⁹ After calculating the IC₅₀ values and looking at the % viability-concentration graph, we discovered that the ligands had greater IC50 values than the equivalent Re(I) complexes. The IC₅₀ values for the Re(I) complexes are between 92.62 to 110.04 µg/mL, while those for the tryptanthrin-based ligands are between 142.54 to 175.81 μ g/mL. The fact that the complex \mathbb{C}^6 had the lowest IC₅₀ value is noteworthy, and this is because of the presence of chlorine group on the tryptanthrin ring. The complexes show the IC₅₀ values that closely resemble that of cisplatin (80.00 $\mu g/mL$) and outperform the effectiveness of the widely used medication carboplatin (165.28 μg/mL), indicating that the molecule has a moderate level of cytotoxicity. 70,71 IC₅₀ of the ligands L^1-L^6 and Re(I) complexes C^1 – C^6 is shown as a bar plot (Figure 8).

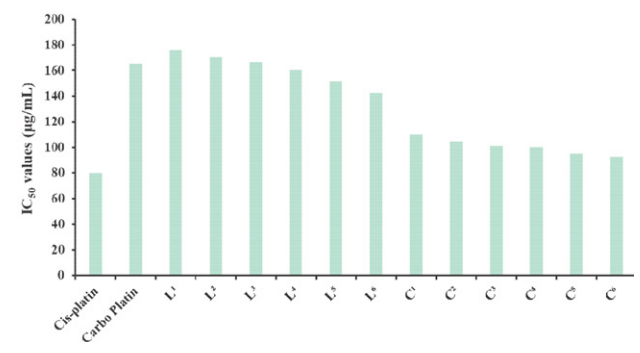


Figure 8. IC₅₀ of the ligands L¹-L⁶ and Re(I) complexes C¹-C⁶.

3. 8. Antibacterial Activity

To combat infectious diseases, it is crucial to control the growth of microorganisms, and this requires effective antibacterial agents. The potency of a newly synthesized molecule against various microorganisms can be assessed by measuring its antibacterial activity. Nutrient agar is commonly used to culture bacteria, and DMSO is used to prepare the testing compound's solution.⁷² Non-turbid results shows that the specific concentration of the tested compound inhibits the growth of the microorganism.⁷³

The antibacterial activity of complexes C⁵ and C⁶ is noteworthy and attributed to the presence of 3 and 4 chlorine atoms, respectively, in their aromatic moiety, which may have an electron-donating effect.⁷⁴ Moreover, metal complexes tend to exhibit higher antibacterial activity than their ligands, possibly due to the activation of the ligand by the metal ion during complex formation and an increase in lipophilicity; it improves medication molecule penetration across the bacterial membrane.^{69,75,76} The compounds' MIC (minimum inhibitory concentration) values are displayed in a bar graph in Figure 9. It is evident that complexes C⁵ and C⁶ have lower MIC values than the other compounds, indicating their stronger antibacterial activity.

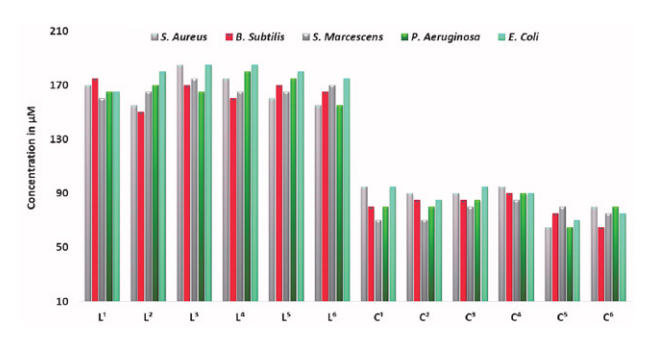


Figure 9. The MIC values for each compound displayed as a bar plot.

3. 9. Cytotoxicity on Brine Shrimp

Brine prawns are an essential component of fish's diet. These small creatures will be studied in a test tube because of their brief seven-day life cycle. They are commonly used to test the cytotoxicity of chemicals on marine species because of their extraordinary ability to thrive in a variety of environmental situations. This research makes use of lab-grown *Artemia cysts*. Analyzing the graph of the mortality percentage versus the logarithm of concentration allows one to determine a substance's lethal concentration (LC_{50}). The minimum concentration necessary to kill 50% of the prawn population under study is known as the lethal concentration. 49,51

Compound C^6 has a lower LC_{50} value because it contains a four-chlorine (-Cl) group, which indicates that it is more cytotoxic than other synthesized compounds. The chlorine substituent, which raises the compounds' lipophilicity and therefore raises its permeability, is to blame for this increased cytotoxicity. All compounds have LC_{50}

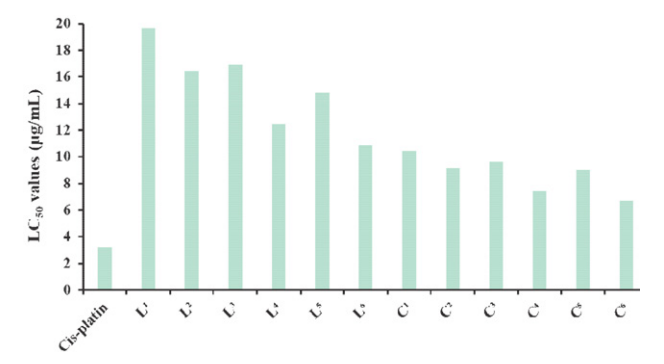


Figure 10. The LC₅₀ data of the synthesized compounds on *Artemia cysts*.

values that are higher than the widely used anticancer drug, cisplatin ($LC_{50} = 3.16 \mu g/mL$). However, compound C^6 has an LC_{50} value that is rather closer to cisplatin (Figure 10).

4. Conclusion

UV-Vis absorption titration, and docking assays showed that the synthesised compounds had a high affinity for CT-DNA and participated in intercalation-type binding. The IC₅₀ values for all the compounds against MCF-7 cells in a cellular investigation range from 90 to 176 μg/mL, indicating substantial anticancer activity. The synthesized rhenium(I) complex C^6 shows an IC₅₀ value comparable to that of cisplatin and all rhenium complexes exhibit better IC₅₀ values than carboplatin. The in vitro cytotoxicity tests of synthesized compounds also show how well they work against Artemia cysts. The LC50 values of complex C^6 is closed to the LC_{50} value of cisplatin. The result for the evaluation of the antimicrobial activities on Gram-positive and Gram-negative microorganisms show that all the complexes have better antibacterial activity. According to the ADME analysis all the compounds have an excellent pharmacokinetic profile. DFT simulations reveal that the electronic distribution predominately resides over the metal ion in the HOMO orbital, which is extremely near to the actual results. Notably, the complex C⁶ has substantial antibacterial and anticancer activity and has the lowest HOMO-LUMO energy gap (1.6104 eV).

Acknowledgement

I am very grateful to the CSIR, New Delhi, for a CSIR-JRF. The authors thank the Sardar Patel University's Department of Chemistry for providing them with access to crucial research resources. We also thank the DST-PURSE at Sardar Patel University for helping with the LC-MS analysis. The authors further acknowledge the support from the CAS Phase-II and UGC-CPEPA programmes as well as the instrumentation and chemical resources made available by Sardar Patel University in India.

5. References

- I. Yavari, M. Askarian-Amiri, Synth. Commun. 2021, 51(10), 1602–1608.
- 2. L. Si, P. Li, X. Liu, L. Luo, *J. Enzyme Inhib. Med. Chem.* **2016**, *31*, 184–196. **DOI:**10.1080/14756366.2016.1178639
- J. Y. Gao, C. S. Chang, J. C. Lien, T. W. Chen, J. L. Hu, J. R. Weng, *Biomedicines* 2021, 9(11), 1527–1539.
 DOI:10.3390/biomedicines9111527
- M. S. C. Pedras, A. Abdoli, Q. H. To, C. Thapa, *Chem. Biodiversity* 2019, 16(3), e1800579–e1800589.
 DOI:10.1002/cbdv.201800579
- G. M. Shankar, V. V. Alex, A. A. Nisthul, S. V. Bava, S. Sundaram, A. P. Retnakumari, S. Chittalakkottu, R. J. Anto, *Cell Prolif.* 2020, 53(1), 1–14. DOI:10.1111/cpr.12710
- 6. M. Maji, D. Panja, I. Borthakur, S. Kundu, *Org. Chem. Front.* **2021**, *8*(11), 2673–2709. **DOI:**10.1039/D0QO01577F
- C. Teja, K. Ramanathan, K. Naresh, R. Vidya, K. Gomathi,
 F. R. Nawaz, *Polycycl. Aromat. Comp.* 2023, 43(1), 874–894.
 DOI:10.1080/10406638.2021.2021257
- A. N. M. A. Alaghaz, M. E. Zayed, S. A. Alharbi, R. A. A. Ammar, A. Chinnathambi, *J. Mol. Struct.* 2015, 1087, 60–67.
 DOI:10.1016/j.molstruc.2015.01.035
- A. Popov, A. Klimovich, O. Styshova, T. Moskovkina, A. Shchekotikhin, N. Grammatikova, L. Dezhenkova, D. Kaluzhny, P. Deriabin, A. Gerasimenko, A. Udovenko, V. Stonik, *Int. J. Mol. Med.* 2020, 46(4), 1335–1346.
- M. I. Shahin, D. A. Abou El Ella, N. S. M. Ismail, K. A. M. Abouzid, *Bioorg. Chem.* 2014, 56, 16–26.
 DOI:10.1016/j.bioorg.2014.05.010
- R. Guda, R. Korra, S. Balaji, R. Palabindela, R. Eerla, H. Lingabathula, N. R. Yellu, G. Kumar, M. Kasula, *Bioorg. Med. Chem. Lett.* 2017, 27(20), 4741–4748.
 DOI:10.1016/j.bmcl.2017.08.064
- 12. R. Kaur, S. K. Manjal, R. K. Rawal, K. Kumar, *Biomol. Struct.* 2017, *25*, 4533–4552. **DOI:**10.1016/j.bmc.2017.07.003
- 13. S. J. S. Franchi, R. A. de Souza, A. E. Mauro, I. Z. Carlos, L. C. de A. Ribeiro, F. V. Rocha, A. V. de Godoy-Netto, *Acta Chim. Slov.* **2018**, *65*(3), 547–553.
 - **DOI:**10.17344/acsi.2017.4112
- F. V. Rocha, C. V. Barra, S. J. S. Franchi, A. V. G. Netto, A. E. Mauro, R. C. G. Frem, *J. Therm. Anal. Calorim.* 2011, 106(2), 385–389. DOI:10.1007/s10973-010-1239-1
- A. Kamal, B. V. S. Reddy, B. Sridevi, A. Ravikumar, A. Venkateswarlu, G. Sravanthi, J. P. Sridevi, P. Yogeeswari, D. Sriram, *Bioorg. Med. Chem. Lett.* 2015, 25(18), 3867–3872.
 DOI:10.1016/j.bmcl.2015.07.057
- D. A. Abdelrheem, A. A. Rahman, K. N. M. Elsayed, H. R. Abd El-Mageed, H. S. Mohamed, S. A. Ahmed, *J. Mol. Struct.* 2021, 1225, 129245. DOI:10.1016/j.molstruc.2020.129245
- A. S. El-Tabl, F. A. El-Saied, W. Plass, A. N. Al-Hakimi, Spectrochim. Acta A Mol. Biomol. Spectrosc. 2008, 71(1), 90–99.
 DOI:10.1016/j.saa.2007.11.011
- A. S. El-Tabl, F. A. El-Saied, A. N. Al-Hakimi, *Transit. Met. Chem.* 2007, 32(6), 689–701.
 DOI:10.1007/s11243-007-0228-0

- A. S. El-Tabl, M. Mohamed Abd El-Waheed, M. A. Wahba,
 N. Abd El-Halim Abou El-Fadl, *Bioinorg. Chem. Appl.* 2015, 2015, 126023–126036. DOI:10.1155/2015/126023
- Y. Li, S. Zhang, R. Wang, M. Cui, W. Liu, Q. Yang, C. Kuang, Bioorg. Med. Chem. Lett. 2020, 30(11), 127159.
 DOI:10.1016/j.bmcl.2020.127159
- 21. E. H. El-Sayed, K. S. Mohamed, *Polycycl. Aromat. Comp.* **2021**, 41(5), 1077–1093. **DOI**:10.1080/10406638.2019.1653941
- H. Luo, C. T. Vong, H. Chen, Y. Gao, P. Lyu, L. Qiu, M. Zhao,
 Q. Liu, Z. Cheng, J. Zou, P. Yao, C. Gao, J. Wei, C. O. L. Ung,
 S. Wang, Z. Zhong, Y. Wang, Chin. Med. (United Kingdom)
 2019, 14(1), 1–58.
- A. H. Mane, A. D. Patil, S. R. Kamat, R. S. Salunkhe, *ChemistrySelect* 2018, 3(23), 6454–6458.
 DOI:10.1002/slct.201800677
- 24. Z. Sadeghian, M. Bayat, F. Safari, *Med. Chem. Res.* **2022**, 31(3), 497–506. **DOI:**10.1007/s00044-022-02856-4
- M. P. Dhaduk, R. A. Dabhi, B. S. Bhatt, V. D. Bhatt, M. N. Patel, *Mater. Today Proc.* 2022, 65, 221–228.
 DOI:10.1016/j.matpr.2022.06.119
- S. C. Lemos, S. J. S. Franchi, A. V. G. Netto, A. E. Mauro, O. Treu-Filho, R. C. G. Frem, E. T. De Almeida, C. Torres, *J. Therm. Anal. Calorim.* 2011, 106(2), 391–397.
 DOI:10.1007/s10973-011-1494-9
- W. H. Mahmoud, R. G. Deghadi, G. G. Mohamed, *Appl. Organomet. Chem.* 2018, 32(4), 1–22. DOI:10.1002/aoc.4289
- W. H. Mahmoud, N. F. Mahmoud, G. G. Mohamed, J. Organom. Chem. 2017, 848, 288–301.
 DOI:10.1016/j.jorganchem.2017.08.001
- A. N. M. A. Alaghaz, H. A. Bayoumi, Y. A. Ammar, S. A. Aldhlmani, *J. Mol. Struct.* 2013, *1035*, 383–399.
 DOI:10.1016/j.molstruc.2012.11.030
- A. N. M. A. Alaghaz, Y. A. Ammar, H. A. Bayoumi, S. A. Aldhlmani, *J. Mol. Struct.* 2014, *1074*, 359–375.
 DOI:10.1016/j.molstruc.2014.05.078
- Y. Kaddouri, B. Bouchal, F. Abrigach, M. El Kodadi, M. Bellaoui, R. Touzani, *J. Chem.*, 2021, 2021, 1–11.
 DOI:10.1155/2021/6663245
- 32. M. N. Patel, P. A. Dosi, B. S. Bhatt, V. R. Thakkar, *Spectrochim. Acta A Mol. Biomol. Spectrosc.* **2011**, *78*(2), 763–770. **DOI:**10.1016/j.saa.2010.11.056
- M. N. Patel, B. S. Bhatt, P. A. Dosi, Spectrochim. Acta A Mol. Biomol. Spectrosc. 2013, 110, 20–27.
 DOI:10.1016/j.saa.2013.03.037
- A. F. Shoair, A. A. El-Bindary, N. A. El-Ghamaz, G. N. Rezk, J. Mol. Liq. 2018, 269(ii), 619–638.
 DOI:10.1016/j.molliq.2018.08.075
- 35. P. R. S. Devi, S. T. David, C. Joel, R. B. Bennie, S. D. Abraham, *Ind. J. Chem. A* **2021**, *60*(11), 1416–1426.
- 36. Y. L. Sang, X. S. Lin, *Acta Chim. Slov.* **2019**, *66*(1), 168–172. **DOI:**10.17344/acsi.2018.4749
- M. Jayasree, R. S. Aparna, R. R. Anjana, J. S. Anjali Devi, N. John, K. Abha, A. Manikandan, S. George, *Anal. Chim. Acta* 2018, 1031(iii), 152–160. DOI:10.1016/j.aca.2018.05.026
- 38. R. R. Varma, J. G. Pandya, F. U. Vaidya, C. Pathak, B. S: Bhatt, M. N. Patel, *Acta Chim. Slov.* **2020**, *67*(3), 957–969.

- DOI:10.17344/acsi.2020.6017
- P. S. Karia, P. A. Vekariya, A. P. Patidar, D. N. Kanthecha, B.
 S. Bhatt, M. N. Patel, *Acta Chim. Slov.* 2019, 66(4), 944–949.
 DOI:10.17344/acsi.2019.5159
- N. Singh, N. Kumar, G. Rathee, D. Sood, A. Singh, V. Tomar,
 S. K. Dass, R. Chandra, ACS Omega 2020, 5(5), 2267–2279.
 DOI:10.1021/acsomega.9b03479
- J. V. Mehta, S. B. Gajera, M. N. Patel, Spectrochim. Acta A Mol. Biomol. Spectrosc. 2015, 136, 1881–1892.
 DOI:10.1016/j.saa.2014.10.103
- 42. E. H. El-Sayed, A. A. Fadda, J. Heterocycl. Chem., 2018, 55(10), 2251–2260. DOI:10.1002/jhet.3276
- B. H. Pursuwani, B. S. Bhatt, F. U. Vaidya, C. Pathak, M. N. Patel, *J. Biomol. Struct. Dyn.* 2021, 39(8), 2894–2903.
 DOI:10.1080/07391102.2020.1756912
- D. N. Kanthecha, B. S. Bhatt, M. N. Patel, D. B. Raval, V. R. Thakkar, F. U. Vaidya, C. Pathak, *J. Inorg. Organomet. Polym. Mater.* 2020, 30(12), 5085–5099.
 DOI:10.1007/s10904-020-01618-2
- 45. S. Rishikesan, M. A. M. Basha, *Acta Chim. Slov.* **2020**, *67*(1), 235–245. **DOI**:10.17344/acsi.2019.5379
- R. R. Varma, B. H. Pursuwani, E. Suresh, B. S. Bhatt, M. N. Patel, *J. Mol. Struct.* 2020, 1200, 127068–127079.
 DOI:10.1016/j.molstruc.2019.127068
- 47. R. A. Dabhi, M. P. Dhaduk, V. D. Bhatt, B. S. Bhatt, J. Biomol. Struct. Dyn. 2022, 41(12), 5382-5398.
 DOI:10.1080/07391102.2022.2086176
 48. F. H. Fl-Saved, A. A. Fadda, Acta Chim. Slov. 2018, 65(4).
- 48. E. H. El-Sayed, A. A. Fadda, *Acta Chim. Slov.* **2018**, *65*(4), 853–864. **DOI:**10.17344/acsi.2018.4506
- 49. R. Lalrempuia, A. Stasch, C. Jones, *Chem. Asian J.* **2015**, *10*(2), 447–454. **DOI:**10.1002/asia.201403089
- P. Bhattacharjee, T. Ghosh, S. Sarkar, P. Pandya, K. Bhadra,
 J. Mol. Recognit. 2018, 31(4), 1–16. DOI:10.1002/jmr.2687
- 51. N. Dey, B. Maji, S. Bhattacharya, *Chem. Asian J.* **2018**, *13*(6), 664–671. **DOI**:10.1002/asia.201701795
- S. Ghosh, D. Usharani, S. De, E. D. Jemmis, S. Bhattacharya, *Chem. Asian J.* 2008, 3(11), 1949–1961.
 DOI:10.1002/asia.200800151
- 53. M. P. Dhaduk, R. A. Dabhi, B. S. Bhatt, V. D. Bhatt, M. N. Patel, *Chem. Phys. Impact* **2023**, *7*, 100261. **DOI:**10.1016/j.chphi.2023.100261
- K. Chanawanno, J. T. Engle, K. X. Le, R. S. Herrick, C. J. Ziegler, *Dalton Trans.* 2013, 42(37), 13679–13684.
 DOI:10.1039/c3dt50894c
- 55. G. Balakrishnan, T. Rajendran, K. Senthil Murugan, M. Sathish Kumar, V. K. Sivasubramanian, M. Ganesan, A. Mahesh, T. Thirunalasundari, S. Rajagopal, *Inorg. Chim. Acta* 2015, 434(I), 51–59. DOI:10.1016/j.ica.2015.04.036
- A. Núñez-Montenegro, R. Carballo, E. M. Vázquez-López, *J. Inorg. Biochem.* 2014, 140, 53–63.
 DOI:10.1016/j.jinorgbio.2014.06.012
- 57. F. A. Cotton, L. M. Daniels, *Cryst. Struct. Commun.* **1983**, 39(11), 1495–1496. **DOI**:10.1107/S0108270183009014
- R. Kia, V. Mirkhani, A. Kálmán, A. Deák, *Polyhedron* 2007, 26(8), 1711–1716. DOI:10.1016/j.poly.2006.12.025
- 59. P. Adwin Jose, M. Sankarganesh, J. Dhaveethu Raja, G. S. Sen-

- thilkumar, R. Nandini Asha, S. J. Raja, C. D. Sheela, *J. Biomol. Struct. Dyn.* **2022**, 40(21), 10715–10729. **DOI**:10.1080/07391102.2021.1947382
- A. Daina, O. Michielin, V. Zoete, Sci. Rep. 2017, 7, 1–13.
 DOI:10.1038/srep42717
- S. Debnath, T. Debnath, S. Bhaumik, S. Majumdar, A. M. Kalle, V. Aparna, *Sci. Rep.* 2019, 9(1), 1–14.
 DOI:10.1038/s41598-019-53376-y
- 62. S. Alam, F. Khan, *J. Biomol. Struct. Dyn.* **2018**, *36*(9), 2373–2390. **DOI**:10.1080/07391102.2017.1355846
- S. Singh, T. Das, M. Awasthi, V. P. Pandey, B. Pandey, U. N. Dwivedi, Biotechnol. Appl. Biochem. 2016, 63(1), 125–137.
 DOI:10.1002/bab.1346
- L. H. Abdel-Rahman, A. M. Abu-Dief, H. Moustafa, A. A. H. Abdel-Mawgoud, *Arab. J. Chem.* 2020, *13*(1), 649–670.
 DOI:10.1016/j.arabjc.2017.07.007
- M. N. Patel, B. S. Bhatt, P. A. Dosi, Appl. Biotechnol. Appl. Biochem. 2012, 166(8), 1949–1968.
 DOI:10.1007/s12010-012-9623-x
- 66. J. Zhu, L. Chen, Y. Dong, J. Li, X. Liu, Spectrochim. Acta A Mol. Biomol. Spectrosc. 2014, 124, 78–83.
- R. R. Varma, J. G. Pandya, J. Sharma, C. Pathak, M. N. Patel, *Mol. Divers.* 2021, 25(2), 687–699.
 DOI:10.1007/s11030-020-10040-2
- 68. N. Shankaraiah, C. Jadala, S. Nekkanti, K. R. Senwar, N. Nagesh, S. Shrivastava, V. G. M. Naidu, M. Sathish, A. Kamal, *Bioorg. Chem.* 2016, 64, 42–50.
 DOI:10.1016/j.bioorg.2015.11.005
- S. Mukherjee, I. Mitra, C. Fouzder, S. Mukherjee, S. Ghosh, U. Chatterji, S. C. Moi, *J. Mol. Liq.* 2017, 247, 126–140.
 DOI:10.1016/j.molliq.2017.09.104
- A. Jamshidvand, M. Sahihi, V. Mirkhani, M. Moghadam, I. Mohammadpoor-Baltork, S. Tangestaninejad, H. Amiri Rudbari, H. Kargar, R. Keshavarzi, S. Gharaghani, *J. Mol. Liq.* 2018, 253, 61–71. DOI:10.1016/j.molliq.2018.01.029
- V. Srinivasan, T. Khamrang, C. Ponraj, D. Saravanan, R. Yamini, S. Bera, M. A. Jhonsi, *J. Mol. Struct.* **2021**, *1225*, 129153.
 DOI:10.1016/j.molstruc.2020.129153
- D. N. Kanthecha, D. B. Raval, V. R: Thakkar, M. N. Patel, *Acta Chim. Slov.* 2018, 65(2), 333–343.
 DOI:10.17344/acsi.2017.4018
- 73. M. N. Patel, P. A. Dosi, B. S. Bhatt, *Acta Chim. Slov.* **2012**, 59(3), 622–631.
- K. Sarkar, P. Dastidar, Chem. Asian J. 2019, 14(1), 194–204.
 DOI:10.1002/asia.201801462
- M. A. Khan, M. Zafaryab, S. H. Mehdi, J. Quadri, M. M. A. Rizvi, *Int. J. Biol. Macromol.* 2017, *97*, 115–122.
 DOI:10.1016/j.ijbiomac.2016.12.090
- M. Eslami Moghadam, A. Jafari, R. Kiani Khashandaragh, A. Divsalar, M. Ghasemzadeh, *J. Iran. Chem. Soc.* 2021, 18(8), 1927–1939. DOI:10.1007/s13738-021-02154-7
- 77. H. M. Parekh, S. R. Mehta, M. N. Patel, *Russ. J. Inorg. Chem.* **2006**, *51*(1), 67–72. **DOI:**10.1134/S003602360601013X
- B. D. Salih, A. H. Dalaf, M. A. Alheety, W. M. Rashed, I. Q. Abdullah, *Mater. Today Proc.* 2020, 43, 869–874.
 DOI:10.1016/j.matpr.2020.07.083

- 79. L. W. Xue, H. J. Zhang, P. P. Wang, *Acta Chim. Slov.* **2019**, 66(1), 190–195. :**OI**:10.17344/acsi.2018.4773
- 80. S. I. Pascu, P. A. Waghorn, B. W. C. Kennedy, R. L. Arrowsmith, S. R. Bayly, J. R. Dilworth, M. Christlieb, R. M. Tyrrell, J. Zhong, R. M. Kowalczyk, D. Collison, P. K. Aley, G. C. Churchill, F. I. Aigbirhio, *Chem. Asian J.* 2010, 5(3), 506–519. DOI:10.1002/asia.200900446
- X. Feng, J. Y. Hu, L. Yi, N. Seto, Z. Tao, C. Redshaw, M. R. J. Elsegood, T. Yamato, *Chem. Asian J.* 2012, 7(12), 2854–2863.
 DOI:10.1002/asia.201200530
- 82. F. U. Ohikhena, O. A. Wintola, A. J. Afolayan, *Int. J. Pharmacol.* **2016**, *12*(7), 701–710. **DOI:**10.3923/ijp.2016.701.710

Povzetek

Sintetizirali smo različne Re(I) organokovinske spojine tipa $[(Re(CO)_3L^{1-6})Cl]$, kjer so ligandi L derivati triptantrina, ter jih karakterizirali z različnimi spektroskopskimi tehnikami. Da bi ugotovili jakost in načine vezave, smo v prisotnosti omenjenih organokovinskih kompleksov izvedli test z DNA telečjega timusa z uporabo absorpcijske titracije in merjenja viskoznosti. Zbrani rezultati kažejo, da gre za interkalacijski tip vezave, kar smo dodatno potrdili s študijami molekulskega sidranja. Švicarsko ADME orodje smo uporabili za izvedbo ADME študije. Osredotočili smo se na izračun energij molekulskih orbital sintetiziranih spojin z uporabo teorije gostotnega potenciala (DFT). Da bi ugotovili morebitne protirakave učinke, smo pripravljene spojine testirali na MCF-7 celični liniji. Ugotovili smo, da so IC_{50} vrednosti naših spojin ekvivalentne vrednostim za standardne učinkovine, kar kaže, da imajo naše spojine podobne antiproliferativne učinke.



Except when otherwise noted, articles in this journal are published under the terms and conditions of the Creative Commons Attribution 4.0 International License